GEOCHEMICAL INVESTIGATIONS OF MIOCENE-INITIATED VOLCANISM OF THE ERCIYES CORRIDOR, CENTRAL ANATOLIA, TURKEY

By Alyssa K. Smith

A Thesis

Submitted in Partial Fulfillment

of the Requirements for the Degree of

Master of Science

in Geology

Northern Arizona University

May 2022

Approved:

Mary R. Reid, Ph.D, Chair

Michael Ort, Ph.D

Nancy Riggs, Ph.D

Paul Umhoefer, Ph.D.

ABSTRACT

GEOCHEMICAL INVESTIGATIONS OF MIOCENE-INITIATED VOLCANISM OF THE ERCIYES CORRIDOR, CENTRAL ANATOLIA, TURKEY

ALYSSA K. SMITH

The Erciyes Corridor lavas erupted from a suite of Miocene stratovolcanoes at the northeastern extent of the Central Anatolian Volcanic Province in central Turkey. Previous workers have hypothesized that volcanism in the Central Anatolian Volcanic Province was initiated by rollback of the Cyprus slab following flat-slab subduction. Recent geochemical investigations have focused predominantly on Quaternary CAVP volcanism, whereas Erciyes Corridor lavas may have accompanied the beginning of slab rollback. New geochemical data are presented here for the Erciyes Corridor lavas, including major and trace elements, Pb and Hf isotopes, and petrographic thin section observations. These data have been used to characterize the Erciyes Corridor volcanoes, to determine potential mantle source components for these centers, and to evaluate how mantle source contributions may have evolved with slab rollback.

Erciyes Corridor lavas range from basalt to dacite (~48 to 67 wt. % SiO_2), with most lavas being evolved (≥ 52 wt. % SiO_2). These lavas are predominantly calc-alkaline, enriched in LREE with respect to HREE, and depleted in HFSE with respect to mantle values. REE patterns of basalts and evolved lavas cross, as represented by lower La/Yb values in basalts as compared to evolved lavas (La/Yb_N ~ 3 to 5 in basalts, ~ 5 to 14 in evolved lavas) at comparable values of Dy/Yb (Dy/Yb_N ~ 1.2 to 1.3 in basalts, ~ 1.0 to 1.3 in the evolved lavas). This, combined with isotopic differences e.g., higher $^{206}Pb/^{204}Pb$, lower Δ7/4, Δ8/4 in some basalts), suggest the Erciyes Corridor basalts were sourced differently from the evolved lavas.

The Erciyes Corridor basalts are similar overall to other basalts from the Central Anatolian Volcanic Province with respect to alkalinity and mantle-normalized trace element patterns. Subtle trace element differences, such lower Th/Yb, Nb/Yb, Ce/Y, and higher Zr/Nb, distinguish the Erciyes Corridor basalts from other Central Anatolian Volcanic Province basalts. Values for these ratios show that the Erciyes Corridor basalts likely were sourced predominantly from a depleted, MORB-like upper mantle under Central Anatolia with lesser contribution from a sediment-modified mantle component.

Evolved Erciyes Corridor lavas can be subdivided into two groups based on their isotopic characteristics. Group 1 lavas have lower Δ7/4 and Δ8/4 values and a narrow range in ε_{Hf} values, which could reflect differentiation via closed type-system crystal fractionation with negligible crustal contamination. Modeling shows that Group 1 dacitic compositions could potentially be derived from Group 1 basaltic andesites via crystal fractionation of a mineral assemblage containing plagioclase, orthopyroxene, clinopyroxene, and hornblende ± small amounts of apatite or titanite. Alternatively, Group 1 evolved lavas may have been derived from basaltic melts similar to those in other Central Anatolian eruptive centers. Group 2 lavas may have been generated by fractionation of the same mineral assemblage, accompanied by crustal assimilation.

If, as proposed, the evolved Group 1 lavas differentiated in a nearly closed system, these same trace element ratios show that their mantle source was dominated by a sediment-modified upper mantle component. Significantly, the Erciyes Corridor basalts do not require incorporation of a deeper, OIB-like intraplate-like mantle component, in contrast to some Quaternary basalts from the Central Anatolian Volcanic Province. The predominance of the ambient upper mantle component and lack of the deeper component in the Miocene-aged Erciyes Corridor lavas could reflect early stages of flat slab rollback in Central Anatolia; incorporation of the deeper component in younger lavas could then represent the progression of rollback-driven convection over time.

ACKNOWLEDGEMENTS

I could write as many pages thanking the amazing people in my life who have helped me along the way as I wrote about the science, so I will keep things short.

Thank you endlessly to my committee members, Dr. Michael Ort, Dr. Nancy Riggs, and the late, great Dr. Paul Umhoefer. A special thank you to my advisor and committee chair, Dr. Mary Reid. I have learned so much under your guidance and I will take all of these lessons forward in my doctor research and beyond.

Thank you to my graduate cohort, my graduate instructors, and to all of my professors from my undergraduate work. No one accomplishes anything alone. You are all proof of that.

Thank you, thank you, thank you to my family and friends who have supported me in my many dreams. You all inspire me and help me to reach farther and dream bigger. A special call out goes to my mom, who has reminded me that success is a product of determination, not just of destiny. Lastly, thank you to my partner and love of my life, Kyle, who has supported me in every way possible. Words will never express my gratitude.

TABLE OF CONTENTS

LIST OF TABLES

LIST OF FIGURES

DEDICATION

This thesis is dedicated to my dogs, Zelda and Andre, who were there for me when no one else could be. Zelda especially was there during the worst parts of the pandemic lockdown. She ensured that I got outside and kept my spirits up while the world around me felt so uncertain.. I could not have accomplished this without their love. Both of my dogs are rescues, but they have rescued me in so many, many ways.

Through dogs, all things are possible.

CHAPTER 1—INTRODUCTION

1.1 Post-collisional volcanism in Central Anatolia

Central Anatolia has been undergoing a complex transition since the Early Miocene, from collision between Eurasia, Arabia, and Africa to transtension as convergence waned (e.g., Şengör and Yilmaz, 1981). At present, convergence between the Arabia and Eurasia plates in Eastern Anatolia, coupled with continued subduction of the Africa plate and accompanying extension in Western Anatolia, is causing rotation and westward extrusion of Central Anatolia (Şengör et al., 2005; Reilinger et al., 2006). Regional magmatism is intimately tied to tectonism (Schleiffarth et al., 2018), and tectonic transitions should be reflected by changes in the chemical compositions of the Miocene to Quaternary volcanic rocks of Central Anatolia.

The most recent period of volcanism in Central Anatolia, responsible for the Central Anatolian Volcanic Province (CAVP), began in the Middle Miocene epoch, and progressed through the Quaternary (Notsu et al., 1995; Toprak, 1998). The volcanic province trends oblique to the Cyprus trench, which is located in the Eastern Mediterranean Sea (Figure 1.1). Volcanism initiated in the northeast, and the distribution of greatest volcanic activity progressively expanded to the southwest (Schleiffarth et al., 2015). Early studies of the CAVP postulate magma genesis occurred via active subduction, predominantly based on proximity to the Cyprus trench and the arc-like geochemical signatures of the lavas, such as large ion lithophile element enrichments and negative high-field strength element anomalies (e.g., Innocenti et al., 1975; Temel et al., 1998). Further studies in regional tectonism and geodynamics, coupled with recognition of subtle differences from arc lavas in the geochemical signatures of lavas, prompted reevaluation of CAVP origins. It is now recognized that active subduction is unlikely to have generated CAVP volcanism (e.g., Sen et al., 2004). Recent hypotheses propose instead that

CAVP volcanism was triggered by the rollback of a horizontally underthrust portion of the Africa plate under Central Anatolia (called the Cyprus slab; Figure 1.1) following ~20 Myr of magmatic quiescence (e.g., Bartol and Govers, 2014; Schleiffarth et al., 2018).

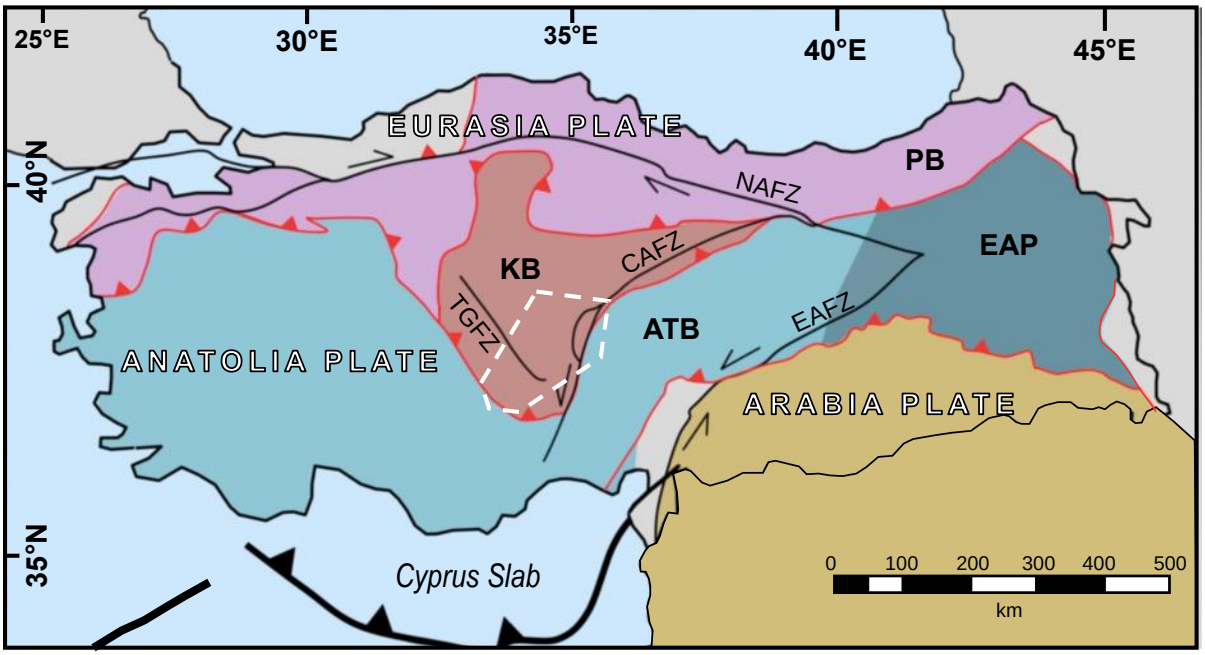

Figure 1.1: Tectonic map of the Eastern Mediterranean region with active plates and tectonic blocks labeled, including the Kirşehir block (KB), Anatolia-Tauride block (ATB), Eastern Anatolia plateau (EAP) and the Pontides block (PB). Suture zones are represented by red barbed lines. Major fault zones are represented by thinner black lines, including the Northern Anatolia fault zone (NAFZ), Eastern Anatolia fault zone (EAFZ), and Tuz Golu fault zone (TGFZ). Trenches are denoted in thick lines with barbs. Dashed white line shows region encompassed by Figure 2.1 in Chapter 2. Figure after Schleiffarth et al. (2017).

1.2 Motivation for this study

Geochemical investigations have been conducted on predominantly Pliocene through Quaternary CAVP lavas, including stratovolcanoes Mt. Erciyes and Mt. Hasan, and the region's numerous monogenetic fields. Few geochemical studies have focused on earlier eruptions that may have accompanied the onset of slab rollback. The Erciyes Corridor is a recently penned name for a collection of seven Miocene- to Pliocene-initiated stratovolcanoes that flank the Kayseri-Yeşilhisar basin through which Mt. Erciyes erupted (Figure 1.2). These volcanoes are

distinctly separated in time from the Quaternary Mt. Erciyes, despite their geographic proximity. According to recent $^{40}Ar/^{39}Ar$ dating, Erciyes Corridor volcanism began at Erkilet volcano by 11.6 ± 0.5 Ma, with the youngest volcanism initiated at Koç Dağ volcano by 3.7 ± 0.4 Ma (Schleiffarth, 2018). Workers such as Innocenti et al. (1975) and Toprak (1998) have suggested that the location of these volcanic centers was controlled by left-lateral motion along the Eçemis fault, eventually forming the Kayseri-Yeşilhisar basin after 2.7 Ma (Figure 1.2). Mt. Erciyes then erupted in the Kayseri-Yeşilhisar basin by ~2.5 Ma (Notsu et al., 1995). Characterizing the Erciyes Corridor lavas and comparing their geochemical signatures to those from other studied CAVP volcanic centers provide an opportunity to look for both spatial and temporal changes in regional magmatism.

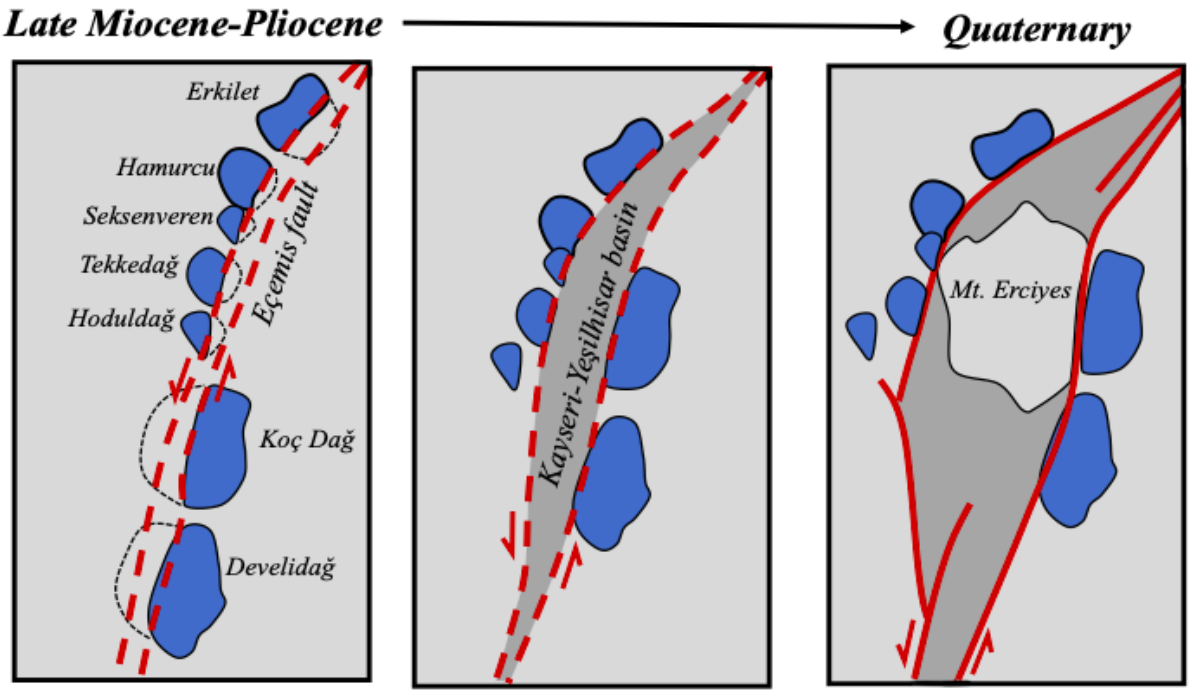

Figure 1.2: Illustration of left-lateral motion along the Eçemis fault since Late Miocene times, (after Toprak, 1998). Dashed lines outline possible portions of the volcanoes prior to opening of the Kayseri-Yeşilhisar basin. The Eçemis fault is interpreted to be younger than initiation of Koç Dağ and Develidağ but volcanism at these centers may have continued after it developed (Innocenti et al., 1975; Toprak, 1998).

Variability in major and trace element characteristics, mineralogy, and isotopic compositions of lavas erupted throughout the CAVP has been interpreted to reflect variable contributions from two or more mantle endmembers. Studies have called upon contributions from an enriched MORB-like upper mantle that hosts regions metasomatized by earlier subduction processes (Deniel et al., 1998; Kürkçüoglu et al., 1998; Kuscu and Genelli, 2011; Reid et al., 2017). Additionally, some studies have suggested that a deeper, ocean island basalt-like "asthenospheric" component could explain certain major and trace element characteristics, particularly in the more alkali-rich basalts (Kürkçüoglu et al., 1998; Reid et al., 2017). The contributions from these different mantle components in erupted lavas could reflect the tectonic

processes active at the time of eruption. Because the Erciyes Corridor lavas are older than those in most other areas of the CAVP, they provide an opportunity to investigate whether mantle source contributions to the CAVP have evolved over time. Changes in source contributions may reflect changes in large-scale tectonic processes, including the influence of slab rollback.

Recent studies have proposed that flat slab subduction, triggered by rapid convergence of the Anatolia plate towards the subducting Africa plate, was responsible for a period of reduced magmatic flux in Central Anatolia from 40 through 20 Ma (Bartol and Govers, 2014; Schleiffarth et al., 2018; Figure 1.3). Slab rollback may have then been the result of slowing convergence rates, which allowed the Cyprus slab portion of the downgoing Africa plate to founder into the underlying mantle (e.g., Reilinger et al., 2006). It has been proposed that rollback of the Cyprus slab began in Miocene times and may have been accompanied by delamination of the overriding mantle lithosphere (Bartol and Govers, 2014).

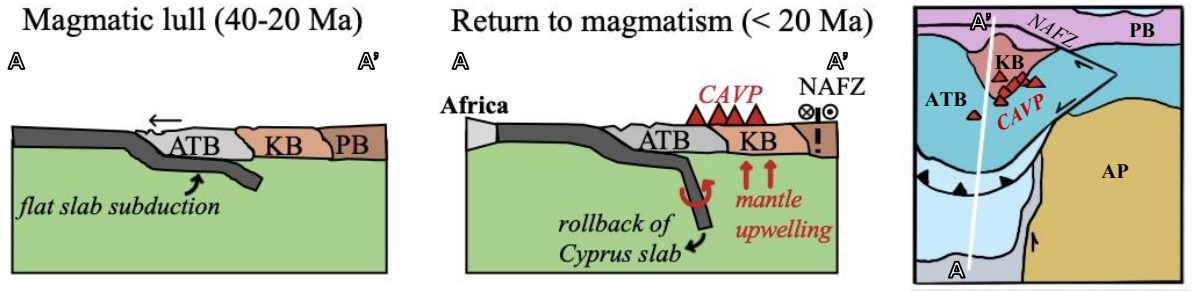

Figure 1.3: Schematic illustration of slab rollback under Central Anatolia after Schleiffarth et al. (2018). Abbreviations include Kirşehir block (KB), Anatolia-Tauride block (ATB), Pontides block (PB), Arabia plate (AP), and Northern Anatolia fault zone (NAFZ). Line A to A' mark on the map view denotes the cross section for the left and center diagrams.

For the Hasan Monogenetic Cluster, a Quaternary volcanic field at the southwestern end of the CAVP (Figure 2.1A), the mantle material that replaced the slab as it rolled back has been interpreted to have been remnant mantle wedge from beneath the Pontides range (Reid et al., 2017); remobilization of the Pontides arc mantle wedge would explain the arc-like geochemical

signatures in the CAVP without requiring active subduction. With time, progressive slab rollback could then allow incorporation of deeper mantle material to fill in behind the foundering slab (Bartol and Govers, 2014; Schleiffarth et al., 2018). If slab rollback triggered Miocene and later volcanism in Central Anatolia, it may have been responsible for temporal changes in relative proportions of source components to the CAVP lavas. The slab rollback model would predict that earlier lavas, such as those in the Erciyes Corridor, should have less of or even lack an asthenospheric component compared to products of later eruptions, e.g., the Hasan Monogenetic Cluster (Reid et al., 2017). Whereas the ideal samples for investigating the model of slab rollback would be near-primary basalts, the majority of the Erciyes Corridor lavas are intermediate to silicic (Schleiffarth, 2018). Certain aspects of these more evolved lavas, such as isotopic ratios and incompatible trace element signatures, may still preserve information about their mantle sources that can be investigated.

The Erciyes Corridor volcanics have been included in stratigraphic studies (Innocenti et al., 1975; Şen et al., 2003), but have not been subject of a comprehensive geochemical investigation. The results presented here include new major and trace element analyses, petrographic thin section characterization, and Pb and Hf isotopic data for the Erciyes Corridor volcanoes. These new data especially expand upon the existing CAVP isotopic dataset, being the third to include whole rock Pb and/or Hf isotopes (Deniel et al., 1998; Reid et al., 2017). This investigation aims to characterize the Erciyes Corridor lavas and compare their chemical compositions to other CAVP volcanic centers. Using these comparisons, it also examines the compositions of the lavas in the context of the slab rollback model.

CHAPTER 2—BACKGROUND AND PREVIOUS WORK

2.1 General geologic history and tectonics

Convergence between Arabia and Eurasia began in Late Cretaceous time, following the closure of the Paleotethys Ocean (Şengör, 1984). Since this time, large-scale changes in tectonism have been marked by cyclic waxing and waning in magmatic flux. This cyclicity of magmatism and its relation to regional tectonism through Central Anatolia was recently investigated as part of the Continental Dynamics-Central Anatolian Tectonics project, funded by the National Science Foundation. The project's investigations have explored regional tectonism and interconnected magmatism in Central and Eastern Anatolia since the Late Cretaceous (Delph et al., 2017; Reid et al., 2017; Portner et al., 2018; Schleiffarth et al., 2018), and have included new geochemical and geophysical data. Analysis of these data have expanded on previous studies of the region and helped to inform recent models for tectonism and magmatism in Central Anatolia.

By the Late Cretaceous time, the region that would later become Central Anatolia existed as a collection of northern Gondwanan platforms separated by ocean basins. Progressive subduction then led to the closing of the Neotethys Ocean (Schleiffarth et al., 2018). The crustal assembly of Anatolia occurred in multiple stages, beginning with the collision of the Kirşehir block and Anatolia-Tauride block against the Pontides block by ~72 Ma (Yilmaz et al., 1997, 2010; Okay et al., 2012). Between ~58 to 40 Ma, subduction dominated greater Anatolia, as evidenced by heightened magmatism throughout the region (Arslan et al., 2013; Parlak et al., 2013). Arabia may have collided with Eurasia in Eastern Anatolia as early as ~50 Ma (Parlak et al., 2013) which, combined with shallowing of the subducted plate under Central Anatolia, may have ultimately led to the cessation of regional magmatism by ~40 Ma (Schleiffarth et al., 2018).

Magmatism returned to the greater Anatolian region by the middle Miocene (LePennec et al., 1994), with eruptions in western Central Anatolia (Karacadağ, Kurt et al., 2008; Galatia Volcanic Province, Wilson et al., 1997) and eastern Central Anatolia (Eastern Taurides, Arger et al., 2000; Reid et al., 2019) as early as 19 Ma. Recent investigations have proposed that rollback of the Cyprus slab was the dominant process responsible for the onset of volcanism in Central Anatolia by middle to late Miocene times (Bartol and Govers, 2014; Schleiffarth et al., 2018). Rollback may have been triggered by slowing convergence rates following flat slab subduction (Jolivet and Faccenna, 2000). The timing for rollback initiation is not well constrained, although current estimates place it at 16 Ma in Central Anatolia (Bartol and Govers, 2014) or potentially earlier (Reid et al., 2019). As the overriding Anatolia Plate is an amalgamation of accreted terranes, the heterogeneous mantle lithosphere associated with it may have become decoupled during flat-slab subduction and foundered with the sinking plate during slab rollback; delamination has additionally been proposed as a mechanism for the ~1 km uplift of the Central Anatolian Plateau (Bartol and Govers, 2014; Delph et al., 2017). Timing of uplift is debated, with estimates as early as ~11 Ma (Meijers et al., 2017) and as late as ~8 Ma (Aydar et al., 2013; Bartol and Govers, 2014). Regardless of the exact timing of these events, it has been hypothesized that upper mantle material would have filled in following rollback and/or delamination of the lithospheric mantle (Bartol and Govers, 2014).

Although active convergence ceased in Central Anatolia in the Miocene epoch, continental convergence and subduction have continued to the present day in Eastern and Western Anatolia respectively; Central Anatolia is the transtensional region caught between the two (Şengör et al, 1985; Abgarmi et al., 2017; Schleiffarth et al., 2018). This transition from compression to extension in Central Anatolia would be required to explain exhumation of the Niğde Massif, just

to the southwest of the Erciyes Corridor (Fayon and Whitney, 2007). New investigations along the Eçemis fault system, 10 – 50 km to the south of the Erciyes Corridor, have placed the local transition to transtensional tectonism even earlier, at 25 – 23 Ma (Umhoefer et al., in review).

GPS measurements (Reilinger et al., 2006) have established the progressive westward extrusion of Central Anatolia, facilitated by movements along the Northern Anatolia Fault Zone (NAFZ) and Eastern Anatolia Fault Zone (EAFZ) that border Central Anatolia to the north and south, respectively (Şengör et al., 1985; Figure 1.1). Convergence between the Arabia and Eurasia plates in Eastern Anatolia has exerted pressure on both the NAFZ and EAFZ, causing Central Anatolia to move westward in a phenomenon known as tectonic escape (Şengör et al., 1985; Reilinger et al., 2006; Gürsoy et al., 2011; Schleiffarth et al., 2018).

At present, the thickness of the crust of Central Anatolia has been estimated at 40 to 30 kilometers based on teleseismic data (Abgarmi et al., 2017). Recent seismic imaging has revealed that the mantle lithosphere under parts of Central Anatolia is thin (< 30 km) or potentially absent based on very slow shear wave velocities (Delph et al., 2017). Delph et al. (2017) attribute these seismically slow shear velocities to a thinned lithospheric lid combined with an influx of hot convecting mantle material at the base of the crust, and correlate areas of thin continental lithosphere with areas of recent volcanism. Although these measurements describe the current state of the lithosphere, recent melt equilibration depth estimates for the Eastern Taurides suggest lithospheric thickness could have been relatively invariant since Miocene time (Reid et al., 2019).

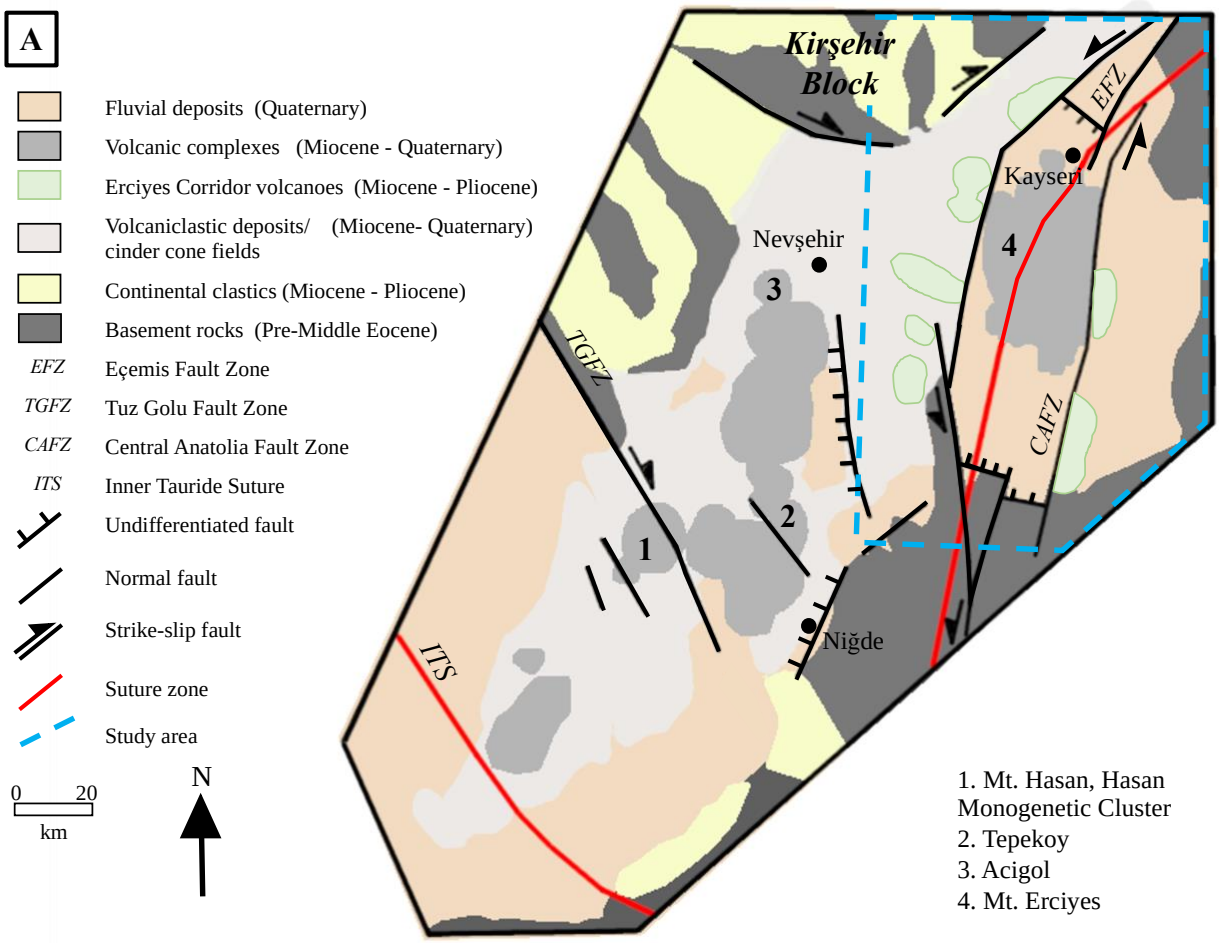
A
Fluvial deposits (Quaternary)
Volcanic complexes (Miocene - Quaternary)
Erciyes Corridor volcanoes (Miocene - Pliocene)
Volcaniclastic deposits/ (Miocene- Quaternary)
cinder cone fields
Continental clastics (Miocene - Pliocene)
Basement rocks (Pre-Middle Eocene)
EFZ Eçemis Fault Zone
TGFZ Tuz Golu Fault Zone
CAFZ Central Anatolia Fault Zone
ITS Inner Tauride Suture
Undifferentiated fault
Normal fault
Strike-slip fault
Suture zone
Study area
0 20
km
N
Kirşehir Block
EFZ
Kayseri
Nevşehir
3
4
TGFZ
CAFZ
2
1
Niğde
ITS
1. Mt. Hasan, Hasan Monogenetic Cluster
2. Tepekoy
3. Acigol
4. Mt. Erciyes

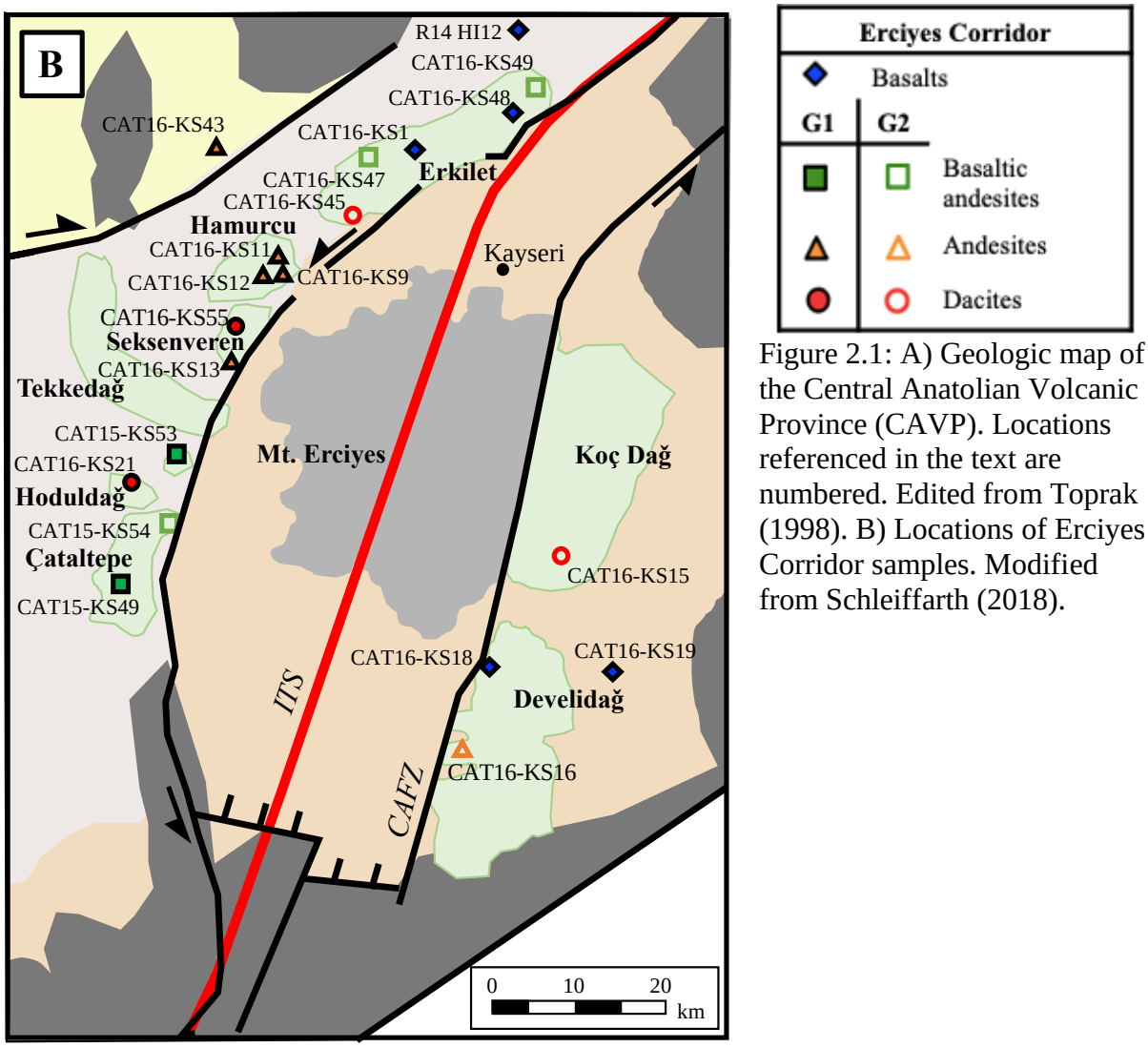

Figure 2.1: A) Geologic map of the Central Anatolian Volcanic Province (CAVP). Locations referenced in the text are numbered. Edited from Toprak (1998). B) Locations of Erciyes Corridor samples. Modified from Schleiffarth (2018).

2.2 Volcanism in the CAVP

The Central Anatolian Volcanic Province (or CAVP) is a 250-km-long chain of volcanic centers in Central Anatolia that has developed since the late Miocene. Volcanic centers in the CAVP include nineteen polygenetic cones and more than 800 monogenetic volcanoes (Toprak, 1998). CAVP lavas are compositionally diverse, from basaltic through rhyolitic with variable alkalinity. Calc-alkaline lavas are most abundant (e.g., Innocenti et al., 1975) with lesser amounts of alkaline lavas (e.g., Kürkcüoglu, 1998; Reid et al., 2017) and rare tholeiitic lavas (e.g., Kürkcüoglu, 2008; Güçtekin and Köprübaşi, 2009).

Monogenetic centers in the CAVP include basaltic lavas (scoria cones and maars) and some silicic lavas (domes). Quaternary basaltic scoria cones compose the bulk of the lavas, though some Miocene to Quaternary andesitic domes can be found in various states of erosion (Toprak, 1998). Rhyolitic monogenetic centers are concentrated around the Acigöl area (southwestern edge of the CAVP; Toprak, 1998), with lavas dated as early as 200 ky and as recent as 20 ky (Schmitt et al., 2011). Basaltic lavas, such as those of the Hasan Monogenetic Cluster (Reid et al., 2017), are calc-alkaline to weakly alkaline whereas centers with bimodal volcanism, such as the Tepekoy Volcanic Province to the east of Mt. Hasan, produced transitional to alkaline basaltic lavas, as well as calc-alkaline evolved lavas (Kuscu and Geneli, 2008; Koralay, 2010).

Of the nineteen polygenetic cones in the CAVP, Mt. Hasan and Mt. Erciyes are the best preserved morphologically (Toprak, 1998) and the best studied. Although both stratovolcanoes had earlier eruptions, the edifices are considered Quaternary features in the literature. Mt. Hasan, or *Hasan Dağı*, erupted in multiple stages, with the earliest lavas beginning at ~13 Ma and subsequent stages continuing through to less than 1 Ma (Deniel et al., 1998). Mt. Hasan lavas are primarily calc-alkaline and span from basaltic to rhyolitic, though later lavas include weakly alkaline basalts (Deniel et al, 1998). Eruptions of Mt. Erciyes, or *Erciyes Dağı*, have been dated to as early as 4.4 Ma and have continued to Holocene times (Notsu et al., 1995; Deniel et al., 1998; Kürkcüoglu et al., 1998; Dogan et al, 2018). Like Mt. Hasan, the lavas are primarily calc-alkaline basalts through rhyolites.

The late Miocene to Pliocene volcanic activity was dominated by an ignimbrite flare-up, deposits of which blanket large swaths of Central Anatolia (Pasquarè, 1968; Innocenti et al., 1975; LePennec et al., 1994; Akin et al., 2021). At least ten voluminous ignimbrites have been

deposited in the region since late Miocene time. Individual ages for these ignimbrites range from 11.2 to 2.7 Ma (Innocenti et al., 1975; Temel, 1992). These deposits are the remnants of caldera-forming eruptions that have since been covered by the volcanic overburden of CAVP eruptions that followed (Akin et al., 2021). CAVP ignimbrites are high in silica (approximately 67 to 80 wt.% SiO_2) and are predominantly calc-alkaline, with few weakly alkaline outliers (Temel et al., 1998; Akin et al., 2021).

Unlike the Quaternary Mt. Hasan and Mt. Erciyes, descriptions of the Erciyes Corridor volcanoes in the existing international literature are limited, although they are described as stratovolcanoes of Miocene-Pliocene age (Innocenti et al., 1975; Toprak, 1998), with the possible exception of Hoduldağ, which was classified as a dome by Toprak (1998). Lavas of the Erciyes Corridor volcanoes have been generally categorized as andesitic (Toprak, 1998). Develidağ volcano is the only center in the Erciyes Corridor that has been subject to a thorough geochemical study (Kürkcüoglu, 2008). Its lavas are characterized as predominantly calc-alkaline basalts through andesites, except for the few that are tholeiitic. Recent $^{40}Ar/^{39}Ar$ dating has determined that the Erciyes Corridor lavas range in age from 3 to ~12 Ma (Table 1; Schleiffarth, 2018). Prior to the Schleiffarth et al. (2017) investigation, only one age had been reported for Erciyes Corridor lavas, that of 5.1 Ma for Tekkedağ based on K-Ar dating (Innocenti et al, 1975).

Table 1: Ages for selected Erciyes Corridor volcanoes

Volcano	**Form[a]**	**Oldest $^{40}Ar/^{39}Ar$ age* (Ma)[b]**	**Youngest $^{40}Ar/^{39}Ar$ age* (Ma)[b]**
Erkilet (west flank)	stratovolcano	11.59 ± 0.52	10.12 ± 0.36
Tekgozkopru (west flank)	stratovolcano	---	---
Hamurcu (west flank)	stratovolcano	9.05 ± 0.08	7.87 ± 0.36
Seksenveren (west flank)	stratovolcano		
Tekkedağ (west flank)[c]	stratovolcano		
Hoduldağ (west flank)	dome ?	7.31 ± 0.16	---
Develidağ (east flank)	stratovolcano	6.23 ± 0.16	2.58 ± 0.09
Çataltepe (west flank)	stratovolcano	5.69 ± 0.05	2.58 ± 0.03
Koç Dağ (east flank)	stratovolcano	3.65 ± 0.36	---

[a] Toprak, 1998
[b] Schleiffarth, 2018
[c] K-Ar dating from Innocenti et al., 1975: 5.1 Ma

2.3 Chemical features of CAVP lavas

The distinction between alkaline and subalkaline lavas used by previous authors is based on their total weight percent alkalis ($K_2O + Na_2O$) compared to their weight percent silica, or total alkais versus silica (TAS) after LeBas et al. (1986). Calc-alkaline lavas typically are enriched in large ion lithophile elements (LILE), such as Rb, K, Sr, and Ba, as well as in Pb, and have distinct negative Nb-Ta anomalies on multielement variation diagrams (Pearce, 1982). The calc-alkaline lavas in the CAVP are enriched in LILE and depleted in high field strength elements (HFSE), such as Nb, Ta, and Ti; ratios between LILE and HFSE are therefore high in these lavas (e.g., Aydin, 2008; Güçtekin and Köprübaşi, 2009). Decoupling of the LILE and HFSE in a lava suite is typically attributed to subduction (Winter, 2013).

Authors of early geochemical studies of CAVP volcanism postulated that volcanism was generated via subduction due to the abundance of calc-alkaline intermediate to silicic lavas (e.g., Innocenti et al., 1975; Temel et al., 1998). This view has fallen out of favor based on geologic evidence and furthered understanding of the tectonic setting in Central Anatolia (e.g., Toprak and

Goncuoglu, 1993). It has been argued that geochemical signatures in Central Anatolian lavas are not reflective of "pure" subduction but are more likely the result of subduction modification of the upper mantle from earlier episodes of subduction (Deniel et al., 1998; Kürkcüoglu et al., 1998; Aydar and Gorgaud, 2002; Kuscu and Geneli, 2011; Reid et al., 2017).

Alkaline lavas are less abundant throughout the CAVP compared to calc-alkaline lavas. CAVP lavas that could be classified as alkaline are often transitional between subalkaline and alkaline (Gencalioglu-Kuscu, 2011; Reid et al., 2017), and mafic to intermediate lavas are typically classified as alkali basalts, basaltic trachyandesites, and trachyandesites, as defined by the TAS classification system by LeBas et al. (1986). Alkaline CAVP lavas have absent to slight negative HFSE anomalies with lower LILE concentrations compared to calc-alkaline CAVP lavas (e.g., Aydin et al., 2008; Güçtekin and Köprübaşi, 2009). The Güçtekin and Köprübaşi (2009) investigation states that high LILE/HFSE ratios in alkaline lavas are suggestive of subduction input and/or crustal contamination. REE diagram patterns for more alkaline lavas resemble those of ocean island basalts (OIB) (Kuscu and Geneli, 2011).

The presence of both calc-alkaline and alkaline lavas throughout the CAVP is significant and has been discussed in context of the tectonic environment in which the lavas were erupted. It has been hypothesized that Central Anatolian lavas have transitioned from calc-alkaline to alkaline over time; this may reflect the transition from collision to transtension/extension in Central Anatolia (e.g., Deniel et al., 1998). This hypothesis has fallen out of favor, and researchers have instead begun to discuss these affinities in regards to mantle sources (e.g., Kuscu and Geneli, 2011; Reid et al., 2017).

2.4 Mantle source components in Central Anatolia

It is imperative to understand the characteristics of mantle components that sourced CAVP lavas, as the geochemical signatures the lavas possess reflect at least in part their mantle sources. The Central Anatolian mantle has long been understood to be heterogeneous (e.g., Notsu et al., 1995), and recent geologic investigations have sought to better constrain potential mantle endmembers. Isotopic heterogeneities in CAVP lavas require at least two distinct mantle components, as best exemplified by near-primary basalts in centers such as the Hasan Monogenetic Cluster (Reid et al., 2017). Isotopic and trace element features in other CAVP lavas, primary or otherwise, may also be explained by these mantle sources, so long as they are not obscured by processes such as crystal fractionation and crustal contamination that could also complicate interpretations of the chemical signatures.

Three mantle components have been identified as contributors to Central Anatolian magmas—an ambient upper mantle (AUM) source, a subduction-modified mantle (SMM), and an intraplate mantle component (IPC); naming conventions for these source components are adopted from the Reid et al. (2017) investigation. While some studies conducted on CAVP lavas have used the terms “lithospheric” and “asthenospheric” as references for melt sources, this thesis refrains from using these distinctions due to the blurring between rheological and geochemical uses of the terms.

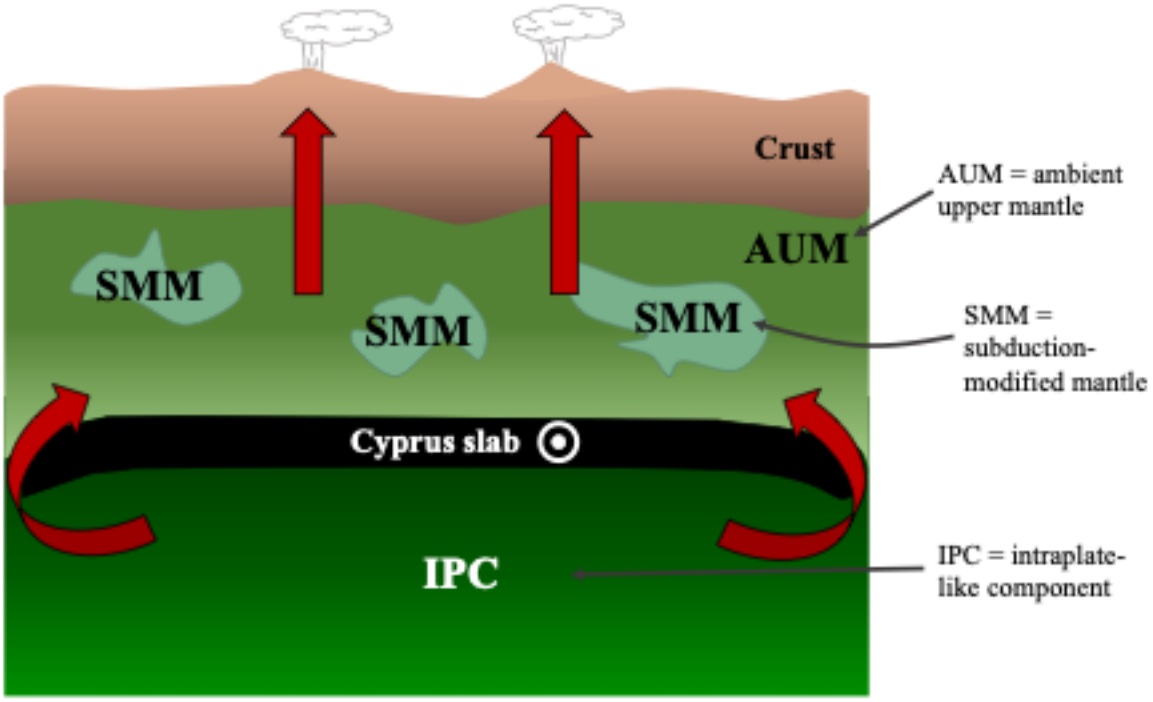

Figure 2.2—Schematic of mantle components under Central Anatolia in the context of the slab rollback model. Uppermost portions of the mantle include an ambient upper mantle (AUM) component, host to regions of subduction-modified mantle (SMM). Bullseye on Cyprus slab signifies slab coming out of the page. Curved red arrows represent flow of lower intraplate component (IPC) around the margins of the sinking Cyprus slab. Vertical red arrows represent ascent of magma through crust. Drawing is not to scale and is meant for visualization only.

2.4.1 Geochemical features of the ambient upper mantle (AUM) and subduction-modified mantle (SMM) components

The ambient and unmodified uppermost portion of the Central Anatolian mantle is interpreted to resemble the source of enriched MORB, or E-MORB (Notsu et al., 1995; Kürkcüoglu, 2008; Reid et al., 2017). Basalts with the least evidence of subduction modification overlap largely with the most enriched portion of MORB fields in isotopic and trace element diagrams (Reid et al., 2017). Trace element characteristics attributed to this component include low La/Sm ($La/Sm_N < 3$, where N signifies normalization to primitive mantle), low Th/Yb (a proxy for mantle metasomatism; Kuscu and Geneli, 2011) and high Th/U (Kürkcüoglu, 2008).

Portions of the Central Anatolian upper mantle have been inferred to have experienced metasomatism from prior episodes of subduction (e.g., Notsu et al., 1995; Aydar and Gourgaud, 2002; Gencalioglu-Kuscu, 2010; Reid et al., 2017; Dogan-Kulahci et al., 2018). Geochemical signatures commonly attributed to subduction, such as LREE and LILE enrichment with respect to N-MORB or primitive mantle values, and negative HFSE anomalies (i.e., negative Nb-Ta anomalies) can be preserved in the mantle, even after subduction terminates (e.g., Kürkcüoglu, 2008; Reid et al., 2017). Mantle metasomatism under Central Anatolia is hypothesized to have been caused by melts of previously subducted sediment, as evidenced by isotopic and chemical similarities between Eastern Mediterranean pelagic sediments and primitive CAVP basalts (Reid et al., 2017).

2.4.2 Geochemical features of a deeper, intraplate-like component (IPC)

While geochemical characteristics of many CAVP lavas can be explained by derivation from ambient upper mantle and subduction-modified mantle sources, a subset of lavas may require contributions from a source comparable to those responsible for OIB (Aydin, 2008; Kuscu and Geneli., 2010; Reid et al., 2017). This intraplate-like source has been identified for Anatolian basalts erupted elsewhere in Anatolia, such as in the study by Parlak et al. (1995). Those basalts, erupted along the Central Anatolian Fault zone to the northeast of the CAVP, have incompatible trace element patterns and REE patterns that very closely resemble those of average OIB compositions. Previous workers have asserted that Quaternary basalts from the Kula region of Western Anatolia best resemble this intraplate-like mantle component, given their OIB-like trace element signatures (e.g., high incompatible element concentrations and lack of Nb-Ta trough) and their Sr and Nd isotopic composition (Alici et al., 2001; Chakrabarti et al., 2012). In the CAVP, the involvement of an OIB-like component is subordinate. An OIB-like

component has been called upon for more alkaline lavas, as exemplified by lavas of the Niğde and Tepekoy volcanic centers (Aydin, 2008; Kuscu and Geneli, 2010), and in the Hasan Monogenetic Cluster basalts (Reid et al., 2017). The Reid et al. (2017) investigation was the first CAVP study to quantify the input from this component, estimating the contribution of the IPC at < 10%. The IPC could be incorporated as melting of the convecting upper mantle as it ascends around the margins of the downgoing slab (Reid et al., 2017; Schleiffarth et al., 2018; Portner et al., 2018). Alternatively, Reid et al. (2017) postulate that an IPC could also be incorporated by mantle convection from "piecemeal" delamination of relict mantle lithosphere following larger delamination associated with slab rollback.

CHAPTER 3: METHODS

Samples were collected during the summers of 2015 and 2016 by Kirk Schleiffarth as part of his dissertation research (Schleiffarth, 2018). Samples were taken throughout the study area to attain good spatial coverage with particular focus on previously uncharacterized volcanic centers. Schleiffarth's sample selection also targeted areas where K-Ar dates are antiquated.

According to Schleiffarth (2018), samples were rinsed in water before a sequence of 5–10-minute ultrasonifications, progressing from dilute hydrogen peroxide (approximately 2%) to dilute hydrochloric acid (approximately 0.1 N), with intermediate and final steps using distilled water. Samples were then powdered for major and trace element analysis. Analyses were performed by X-ray fluorescence spectrometry, inductively-coupled plasma mass spectrometry, and inductively coupled plasma atomic emission mass spectrometry at SGS minerals in Lakefield, Ontario.

Analyses of Hf and Pb isotopes were conducted by Schleiffarth at the Ecole Normale Supérieure in Lyon (ENSL) using the whole-rock powders prepared for the bulk chemical analyses. Approximately 600 mg of the rock powders were leached for a total of 50 minutes in high purity 6 M HCl, alternating between heating to 125°C and ultrasonication. The residue was then washed in ultrapure water before being digested in a 1:3 mixture of doubly-distilled concentrated HNO_3 and HF. Following evaporation, the Hf in the residue was then leached using high-purity, concentrated HF and separated from Ti and Zr using the two-stage chromatographic procedure outlined by Blichert-Toft et al. (1997). Following HF leaching, the Ca-Mg fluorite precipitate was converted to bromides by digestion in 6 M HCl, evaporation to dryness, and dissolution in 1 N HBr. Lead was then removed from this solution using a 500 μL AG 1-X8 anion

exchange resin column. Dilute HBr was used to elute the sample matrix and 6 M HCL was used to elute Pb.

The separated samples were run by Schleiffarth on the Nu Plasma HR multiple-collector inductively coupled mass spectrometer at ENSL. Lead analyses were conducted using Tl doping (5 ppb) and sample standard bracketing after White et al. (2000). The NIST 981 Pb standard was run after every second Pb isotope analysis of the unknowns. The NIST 981 values of Eisele et al. (2003) were used for normalization. 2σ reproducibility for $^{206}Pb/^{204}Pb$, $^{207}Pb/^{204}Pb$, and $^{208}Pb/^{204}Pb$ are ± 100-200 ppm (or 0.01-0.02%) with internal run errors better than external reproducibility. Analyses of the JMC-475 Hf standard were run every after every two to four Hf isotopic analyses. Results were corrected for instrumental mass fractionation using an exponential law relative to $^{179}Hf/^{177}Hf= 0.7325$. Blanks for both Hf and Pb were < 20 pg. The JMC-475 Hf standard yielded $^{176}Hf/^{177}Hf = 0.282158 \pm 0.000004$ (2 standard deviation [sd]; n = 11).

All Erciyes Corridor hand samples large enough to be cut into billets for petrographic thin sections were sent to Quality Thin Sections in Tucson, AZ. A total of nineteen thin sections were made.

CHAPTER 4: RESULTS

4.1 Petrographic sample descriptions

Erciyes Corridor lava samples were classified as basalts through dacites based on phenocryst assemblages (Appendix Table 1). Erciyes Corridor basalts contain plagioclase laths, and subhedral to anhedral crystals of olivine, and pyroxenes with sparse oxides within a holocrystalline groundmass. Crystals range from microlites to phenocrysts up to 1 mm in size. Olivine crystals are commonly rimmed with iddingsite. Most orthopyroxene and clinopyroxene crystals are rimmed with iron oxide. Olivine and pyroxene crystals partially enclose interstitial plagioclase in some samples (subophitic texture). Vesicles, when present, are irregular.

Basaltic andesites contain phenocrysts of plagioclase, clinopyroxene and/or orthopyroxene, and some oxides in holocrystalline to cryptocrystalline groundmass. One basaltic andesite sample also contains iddingsite-rimmed olivine (CAT16-KS49). Phenocrysts are subhedral to anhedral and range in size from <1 mm to 5 mm. Plagioclase occurs as blocky crystals and as fine microlites in the groundmass. Clinopyroxene is frequently twinned.

Andesites contain subhedral to anhedral phenocrysts of plagioclase, orthopyroxene +/- clinopyroxene, and oxides in fine-grained holocrystalline to glassy groundmass. Crystal sizes are on the mm scale; one sample contains glomerocrysts of pyroxenes, plagioclase, and oxides (CAT16-KS16; Figure 4.1). Plagioclase crystals are blocky to elongate with abundant albite twinning. Sieve texture and embayments are common in plagioclase. Clinopyroxene crystals are commonly twinned. Oxides are either distinct crystals within the groundmass or are included in major mineral crystals.

Erciyes Corridor dacites contain plagioclase, hornblende +/- pyroxenes, and oxides. Crystals are on the mm scale, are predominantly subhedral to anhedral and are heavily altered.

Groundmasses are stained by iron oxide and vary from holocrystalline or cryptocrystalline to glassy between individual dacite samples. Plagioclase is the most abundant phase in these lavas and forms blocky, subhedral laths with frequent embayments and rare compositional zoning. Hornblende crystals in these lavas are anhedral to subhedral (rarely euhedral) and heavily altered; variable alteration is evidenced by opacitic rims or entire replacement by opaque minerals. When present, vesicles are irregular.

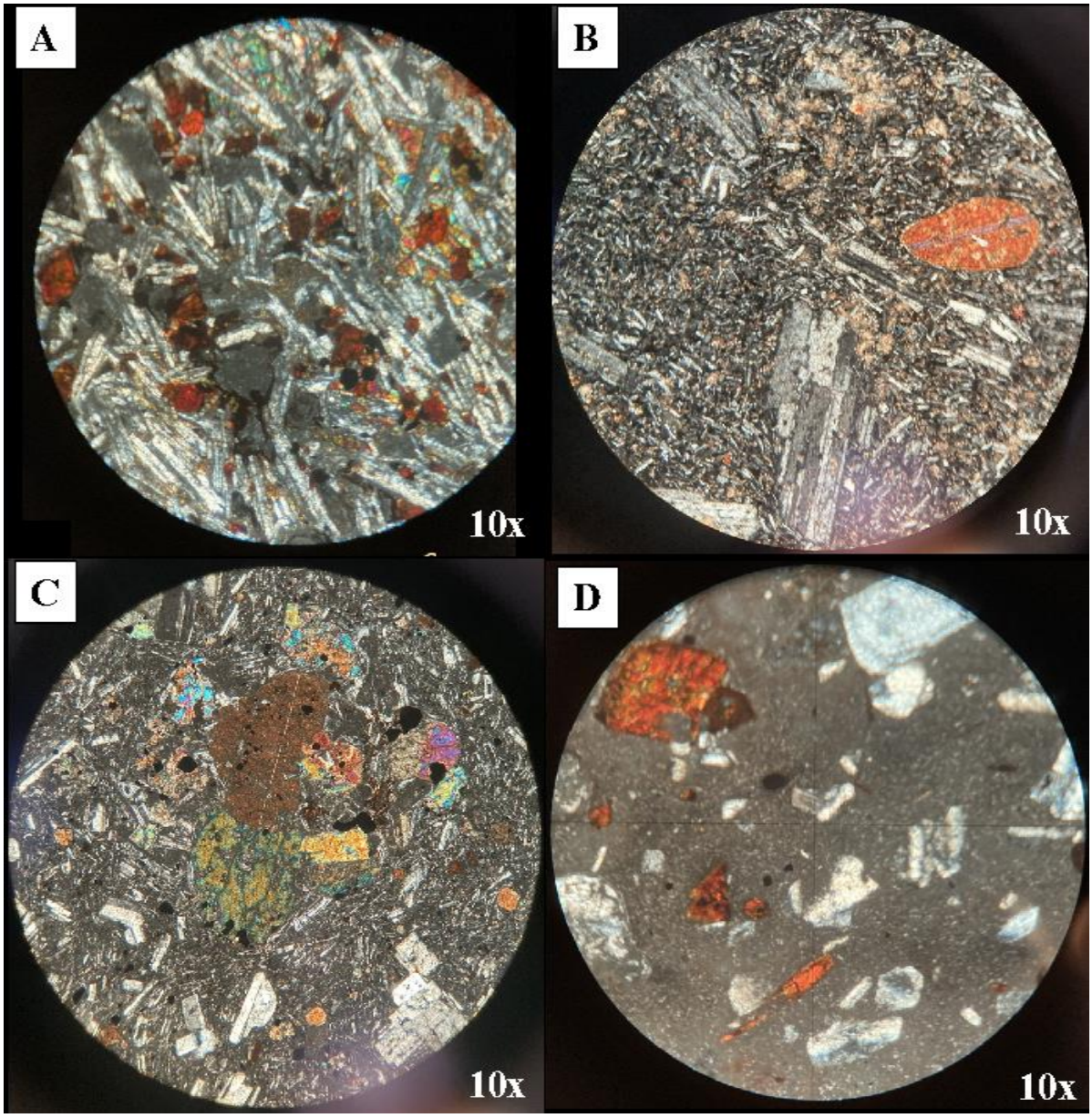

Figure 4.1: Representative thin section images for Erciyes Corridor lavas. A) Basalt (CAT16-KS1): contains lath-like plagioclase and iddingsite-altered olivine crystals with irregular vesiculation. B) Basaltic andesite (CAT15-KS40): contains multiple sizes of elongate plagioclase crystals and both phenocryst and groundmass clinopyroxene. C) Andesite (CAT16-KS16): contains elongate plagioclase crystals, altered clinopyroxene and orthopyroxene, and oxides. D) Dacite (CAT16-KS55): contains blocky plagioclase, heavily altered hornblende, and oxides in a fine-grained groundmass.

4.2 Whole Rock Geochemistry

4.2.1 Geochemistry of the Erciyes Corridor evolved lavas

The Erciyes Corridor lavas range from 49 to nearly 70 wt. % SiO_2; those lavas with a silica content greater than 52 wt. % are identified as "evolved" (basaltic andesite through dacite). By using the classification system of LeBas et al. (1986), the evolved lavas are largely subalkaline, with a few samples classified as transitional to weakly alkaline based on their alkali content ($Na_2O + K_2O$; Figure 4.2A). While the transitional to alkaline evolved lavas could be classified as basaltic trachyandesites and trachyandesites, this thesis groups them with the basaltic andesites and andesites, as no further distinction is made between the different lava types at the same silica content. The subalkaline lavas can further be classified as calc-alkaline (Figure 4.2B).

Major element oxides CaO, MgO, total FeO, TiO_2, and MnO in the evolved lavas decrease with increasing SiO_2, while K_2O increases (Figure 4.3). Concentrations of Al_2O_3 are broadly similar in lavas up to ~ 65 wt. % SiO_2, above which they decrease with increasing silica. Major element concentrations for MnO and Na_2O are moderately variable in the evolved lavas whereas the concentrations of K_2O, FeO(Total) and P_2O_5 are significantly more variable.

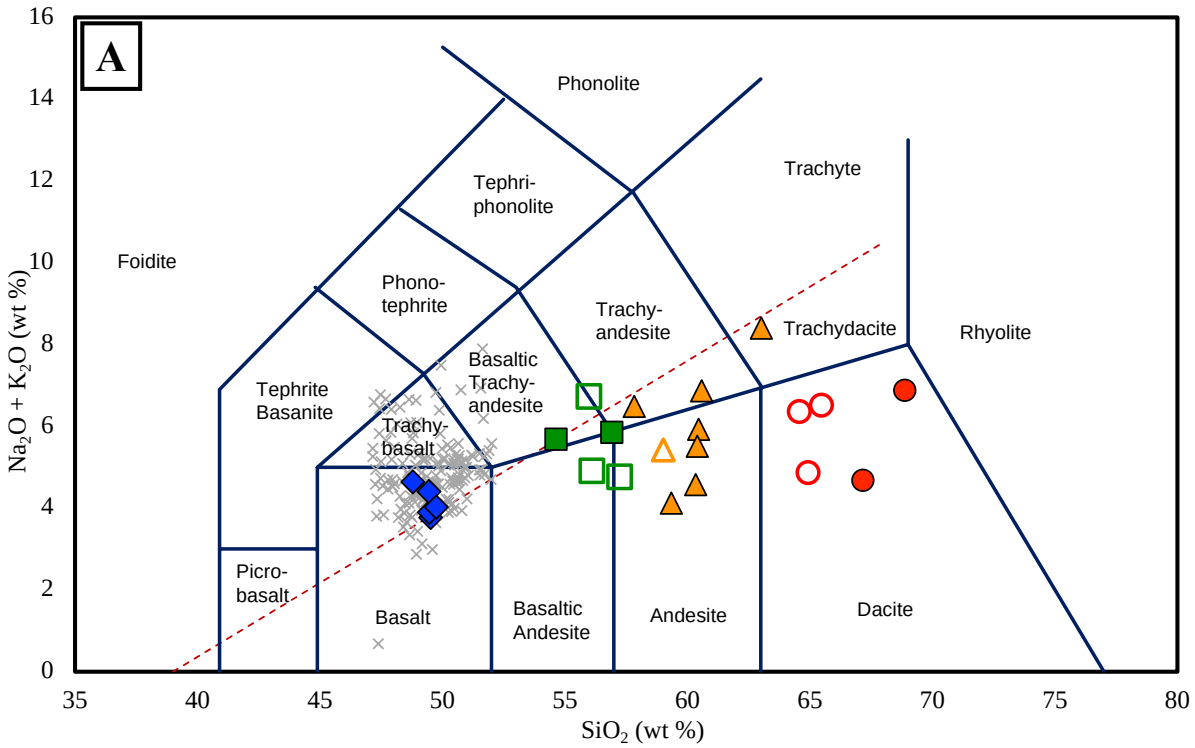

Figure 4.2: (A) Total Alkali vs. Silica (TAS) diagram after LeBas et al. (1986) and (B) AFM diagram for the Erciyes Corridor lavas. Other CAVP lavas (Uslular et al., 2019) are within a constrained silica range (~47-52 wt. % SiO_2). This silica range is most directly comparable to that for the Erciyes Corridor basalts. Designation of evolved lava groups will be further discussed in Section 5.2

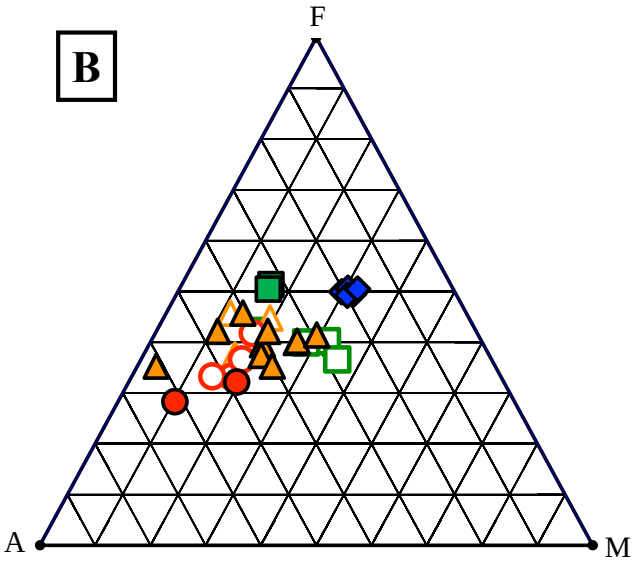

	Group 1 (G1)	Group 2 (G2)
Basalt	◆	
Basaltic andesite	■	□
Andesite	▲	△
Dacite	●	○
CAVP basalts (Uslular et al, 2019)	×	

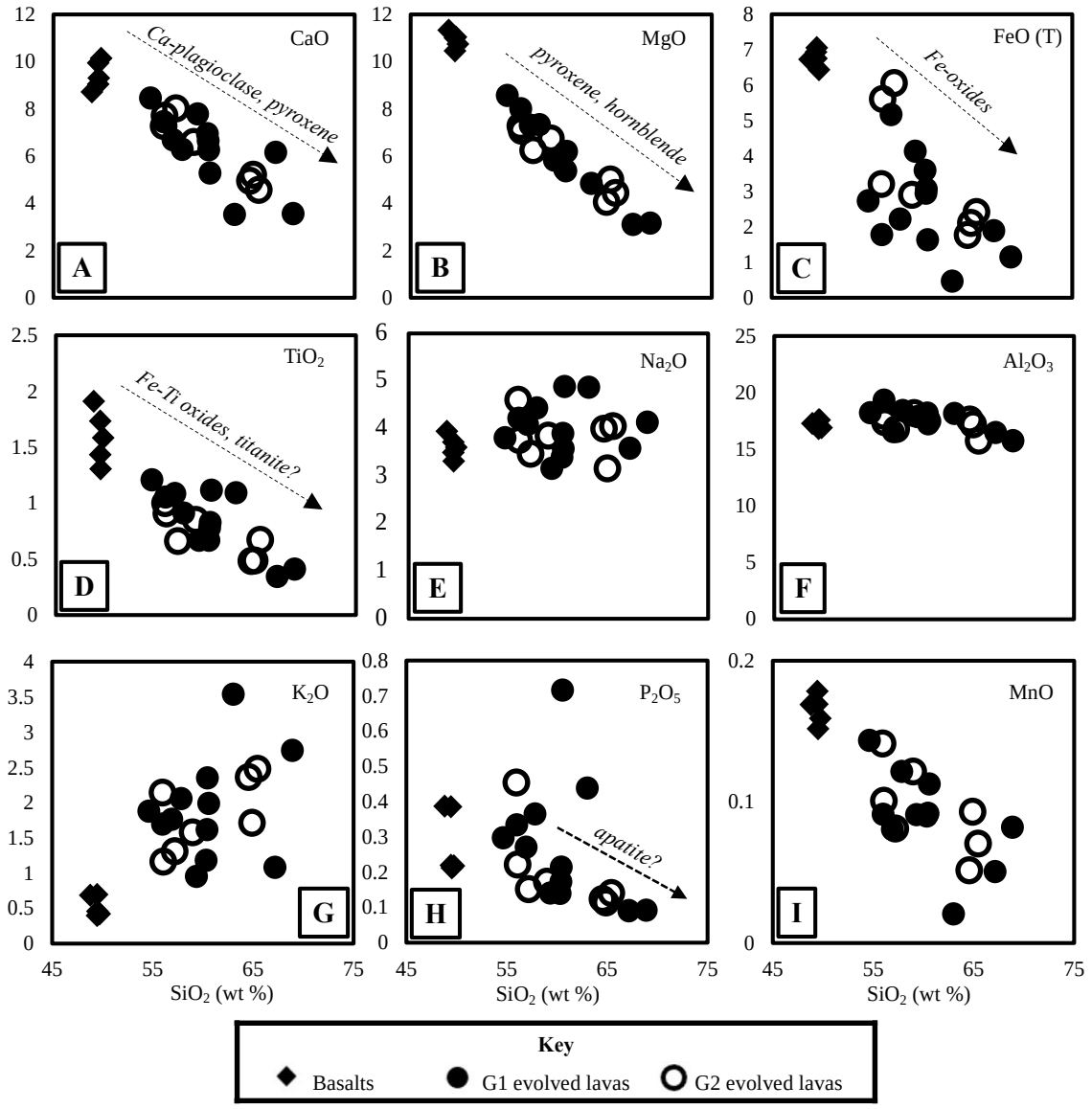

Figure 4.3: (A-I) Major element Harker variation diagrams for Erciyes Corridor lavas. Major element oxides are measured in weight percent. Dashed lines labeled with mineral names illustrate how crystal fractionation might have produced the observed trends in oxide concentrations.

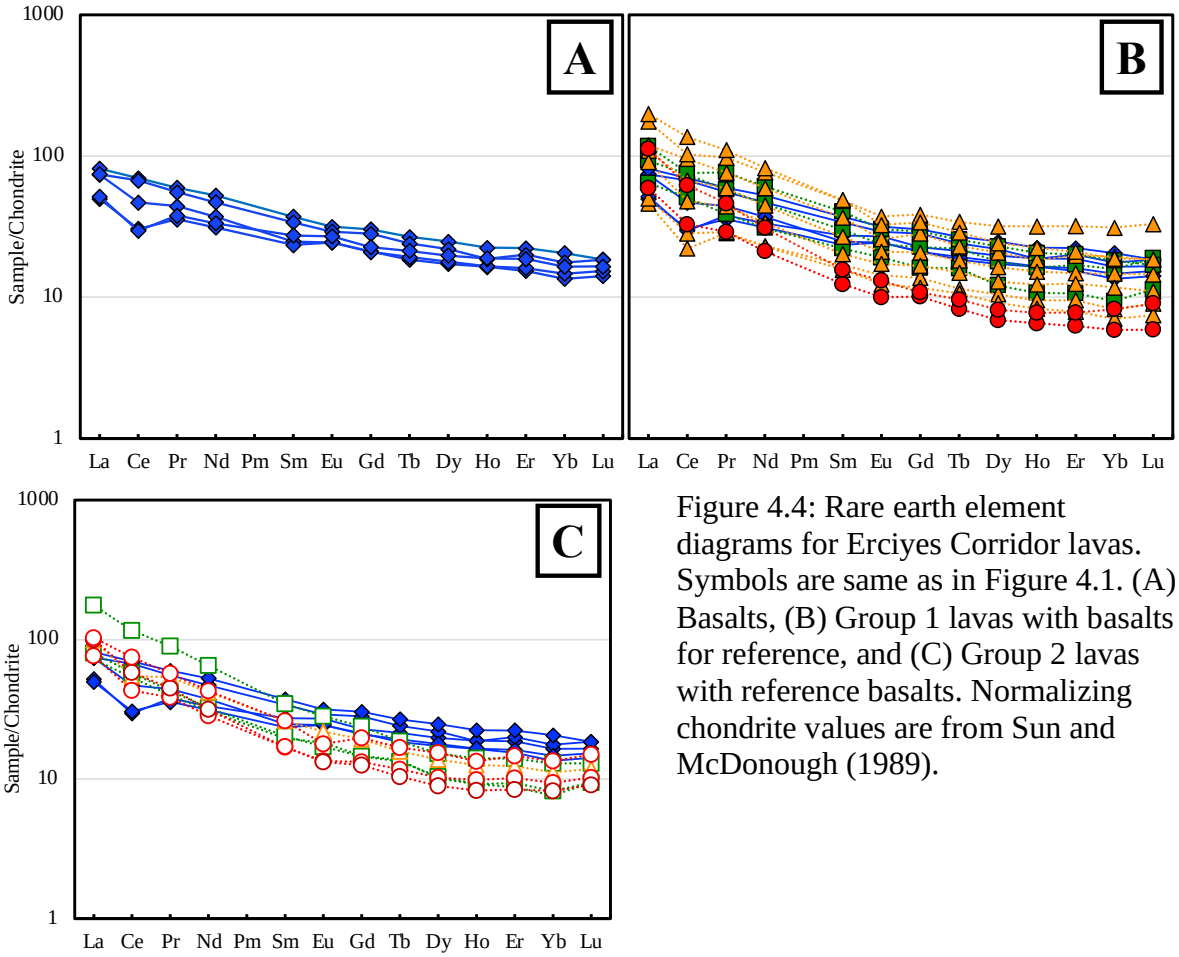

Figure 4.4: Rare earth element diagrams for Erciyes Corridor lavas. Symbols are same as in Figure 4.1. (A) Basalts, (B) Group 1 lavas with basalts for reference, and (C) Group 2 lavas with reference basalts. Normalizing chondrite values are from Sun and McDonough (1989).

The evolved Erciyes Corridor lavas are enriched in LREE with respect to HREE (Figure 4.4). Values for La/Yb_{CN} range from 5.6 to 13.6 and for Dy/Yb_{CN} range from 1.0 to 1.3, where the subscript "CN" signifies normalization to chondritic concentrations (values of Sun and McDonough, 1989). Europium anomalies (Equation 1; Taylor and McLennan, 1985)

Eq. 1

$$\frac{Eu}{Eu*} = \frac{Eu_N}{\sqrt{Sm_{CN} \cdot Gd_{CN}}}$$

in the evolved lavas are moderately negative to slightly positive, ranging from 0.79 to 1.1. Values for Dy/Dy* (Equation 2; Davidson et al., 2013).

Eq. 2

$$\frac{Dy}{Dy*} = \frac{Dy_N}{La_{CN}^{\frac{4}{13}} \cdot Yb_{CN}^{\frac{9}{13}}}$$

can be used to represent the curvature of a REE pattern as single point. Values for Dy/Dy* > 1 signify Dy concentrations elevated from a linear extrapolation between La and Yb on a REE diagram, whereas Dy/Dy* < 1 signify Dy concentrations lower than those predicted by a linear extrapolation. REE patterns for the evolved Erciyes Corridor lavas are concave upwards, and Dy/Dy* values range from 0.44 to 0.75.

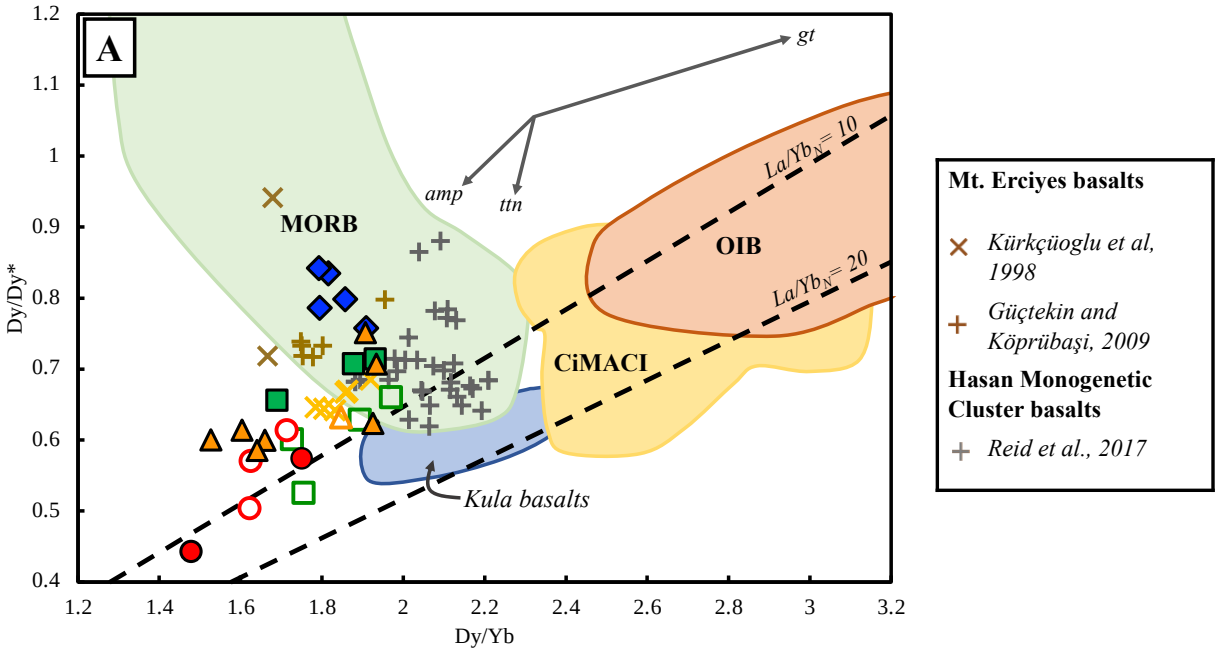

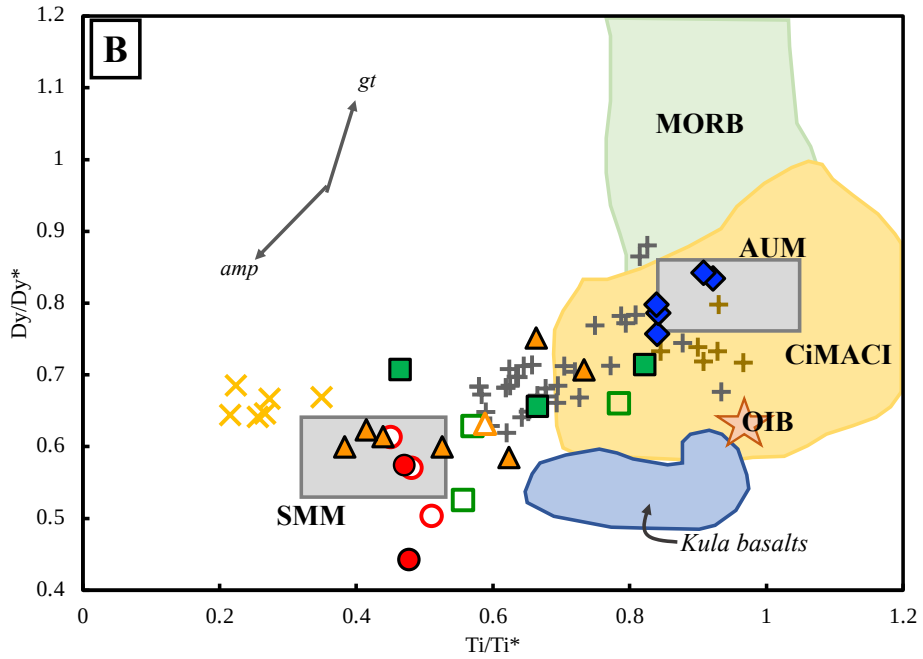

Figure 4.5: Curvature and gradient of Erciyes Corridor REE patterns, represented by Dy/Dy*—Dy/Yb. Also shown: (B) Dy/Dy*—Ti/Ti* after Davidson et al. (2013) and Reid et al. (2017); see equations in text. Symbols as in Figure 4.2 with the addition of yellow x's, which denote proximal Eastern Mediterranean pelagic sediments from Klaver et al. (2015). Labeled polygons for MORB and OIB are those used by Reid et al. (2017); orange star for OIB in (B) is the average composition as reported by Sun and McDonough (1989), circum-Mediterranean anorogenic basalts (CiMACI) from Lustrino and Wilson (2007), and basalts of the Kula region from Chakrabarti et al. (2012) are also included for reference. Gray vectors represent crystallization of 10% garnet (gt), 20% amphibole (amp), and 0.5% titanite (ttn); partition coefficients for amphibole and garnet from Pilet et al. (2011). Titanite partition coefficients used are those reported by Bachmann et al. (2005).

Evolved Erciyes Corridor lavas are enriched in LILE, such as Rb, Ba, Pb, and K, with respect to N-MORB, whereas HFSE concentrations (Nb, Ta, and Ti) are generally lower than in N-MORB (Figure 4.6). Concentrations of trace elements such as La, Dy, and Ni are highly variable (Figure 4.7), which leads to the scatter in their incompatible element patterns. When normalized to N-MORB, ratios of Nb/La range from 0.3 to 0.7. Values for Ti/Ti* (Eq. 3; Reid et al., 2017), a measurement of the Ti anomaly in a lava's incompatible element pattern, range from 0.38 to 0.82 in the evolved lavas (Figure 4.5).

Eq. 3:

$$\frac{Ti}{Ti}^{*} = \frac{Ti_{PM}}{\left(\frac{Sm_{PM} + Gd_{PM}}{2}\right) + \left(\frac{Tb_{PM}}{4}\right)}$$

This study reports new Pb and Hf isotopic data for the Erciyes Corridor; values are presented in Appendix Table 1. Lead isotopic values for the Erciyes Corridor evolved lavas overlap those for the majority of the Hasan Monogenetic Cluster (HMC) basalts (Reid et al., 2017) as well as those of the most proximal Eastern Mediterranean sediments (Klaver et al., 2016) (Figure 4.8). $^{207}Pb/^{204}Pb$ and $^{208}Pb/^{204}Pb$ ratios in the evolved Erciyes Corridor lavas are displaced above the Northern Hemisphere Reference Line (NHRL; Hart, 1984) in these plots. Quantifying this deviation from the NHRL is another way to visualize the Pb isotope data. As presented in the Hart (1984) study, the displacement is calculated as the following, where the subscript "NHRL" refers to NHRL values (Eq. 4) at the same $^{206}Pb/^{204}Pb$ value as an Erciyes Corridor lava of interest (Eq. 5).

Eq. 4:

$$^{207}Pb/^{204}Pb = 0.1084(^{206}Pb/^{204}Pb)_{NHRL} + 13.491$$

$$^{208}Pb/^{204}Pb = 1.209(^{206}Pb/^{204}Pb)_{NHRL} + 15.627$$

Eq. 5:

$$\Delta 7/4 = [(^{207}Pb/^{204}Pb)_{sample} - (^{207}Pb/^{204}Pb)_{NHRL}] \cdot 100$$

$$\Delta 8/4 = [(^{208}Pb/^{204}Pb)_{sample} - (^{208}Pb/^{204}Pb)_{NHRL}] \cdot 100$$

Calculated Δ7/4 and Δ8/4 values for the evolved lavas range from 11.8 to 15.6 and 46.9 to 65.3 respectively.

Hafnium isotopic data are presented as ε_{Hf}, where $^{176}Hf/^{177}Hf$ in the sample is normalized to the value for the chondritic uniform reservoir (CHUR) or 0.282772 (Blichert-Toft and Albarede, 1997).

Eq. 6:

$$\varepsilon_{Hf} = \left[\frac{\left(\frac{176Hf}{177Hf}\right)_{sample}}{\left(\frac{176Hf}{177Hf}\right)_{CHUR}} - 1 \right] \times 10^4$$

Evolved Erciyes Corridor lavas vary in ε_{Hf} from + 2.6 to +10.1, ranging between those measured in the HMC basalts (Reid et al., 2017) and Cappadocian ignimbrites (Akin et al., 2021). There are two distinct populations of ε_{Hf} in the evolved lavas, one with higher, invariant ε_{Hf} values (Group 1) and another with lower, more variable ε_{Hf} values (Group 2). The isotopic dissimilarity of these groups of evolved lavas will be a major focus of the discussion in Section 5.4, as contrasts in their isotopic composition are crucial for understanding their petrogenesis. Values of ε_{Hf} generally decrease with increasing Δ7/4 and Δ8/4 in the evolved lavas.

4.2.2 Geochemistry of the Erciyes Corridor basalts

Erciyes Corridor basalts are transitional to weakly alkaline (Figure 4.2A). Data points for these lavas are clustered together on Harker variation diagrams for CaO, FeO(T), MgO, Al_2O_3, and K_2O (Figure 4.3), but diagrams for TiO_2, MnO, Na_2O, and P_2O_5 values exhibit scatter. Magnesium numbers (Mg#) in the Erciyes Corridor basalts are low, with a median (Mg# of ~39 (Mg# =100*(Mg/(Mg+Fe), calculated in mol); Mg# in primitive basalts are typically > 60 (Winter, 2010). Concentrations of compatible elements, such as Ni and Cr, are variable (Cr = 63 – 237 ppm; Ni= 86 – 128 ppm).

Erciyes Corridor basalts are enriched in LREE with respect to HREE on chondrite-normalized REE diagrams, but to a lesser extent than the majority of the evolved lavas (Figure 4.4). The REE patterns of the basalts are less steep than those of the evolved lavas, as exhibited by lower values of La/Yb_{CN} (3.2 to 5.5, compared to 5.6 to 13.6 in the evolved lavas) despite similar values of Dy/Yb_{CN} (1.2 to 1.3, compared to 1.0 to 1.3 in the evolved lavas). Additionally, Dy/Dy* values in the basalts range from 0.76 to 0.84, compared to lower values in the evolved lavas (0.44 to 0.75), and reflect more concave-upwards REE patterns. These values are within range of values for lavas from the HMC and Mt. Erciyes (Figure 4.5).

Incompatible trace element patterns for Erciyes Corridor basalts, normalized to N-MORB (Sun and McDonough, 1989), feature slight negative HFSE anomalies and positive K and Pb anomalies, with modest positive Sr anomalies (Figure 4.7). These anomalies are much less pronounced in the basalts compared to the evolved lavas. Ti/Ti* values for the basalts range from 0.84 to 0.92, elevated from values in the evolved lavas. Generally, the incompatible trace element patterns in the basalts show less scatter those of the evolved lavas.

Two of the Erciyes Corridor basalts overlap in their paired $^{207}Pb/^{204}Pb$ and $^{206}Pb/^{204}Pb$, and $^{208}Pb/^{204}Pb$ and $^{206}Pb/^{204}Pb$ values with those of the HMC basalts and the most radiogenic of the evolved Erciyes Corridor evolved lavas (Figure 4.8). Values for two other basalts extend to distinctly higher $^{206}Pb/^{204}Pb$ (18.96 to 19.08) with respect to the rest of the measured CAVP lavas. Additionally, Erciyes Corridor basalts range in $\Delta 7/4$ and $\Delta 8/4$ to lower values than those of the evolved lavas (Figure 4.9). Values of ε_{Hf} in the basalts range from +5.6 to +7.7, intermediate to values in the evolved Erciyes Corridor lavas.

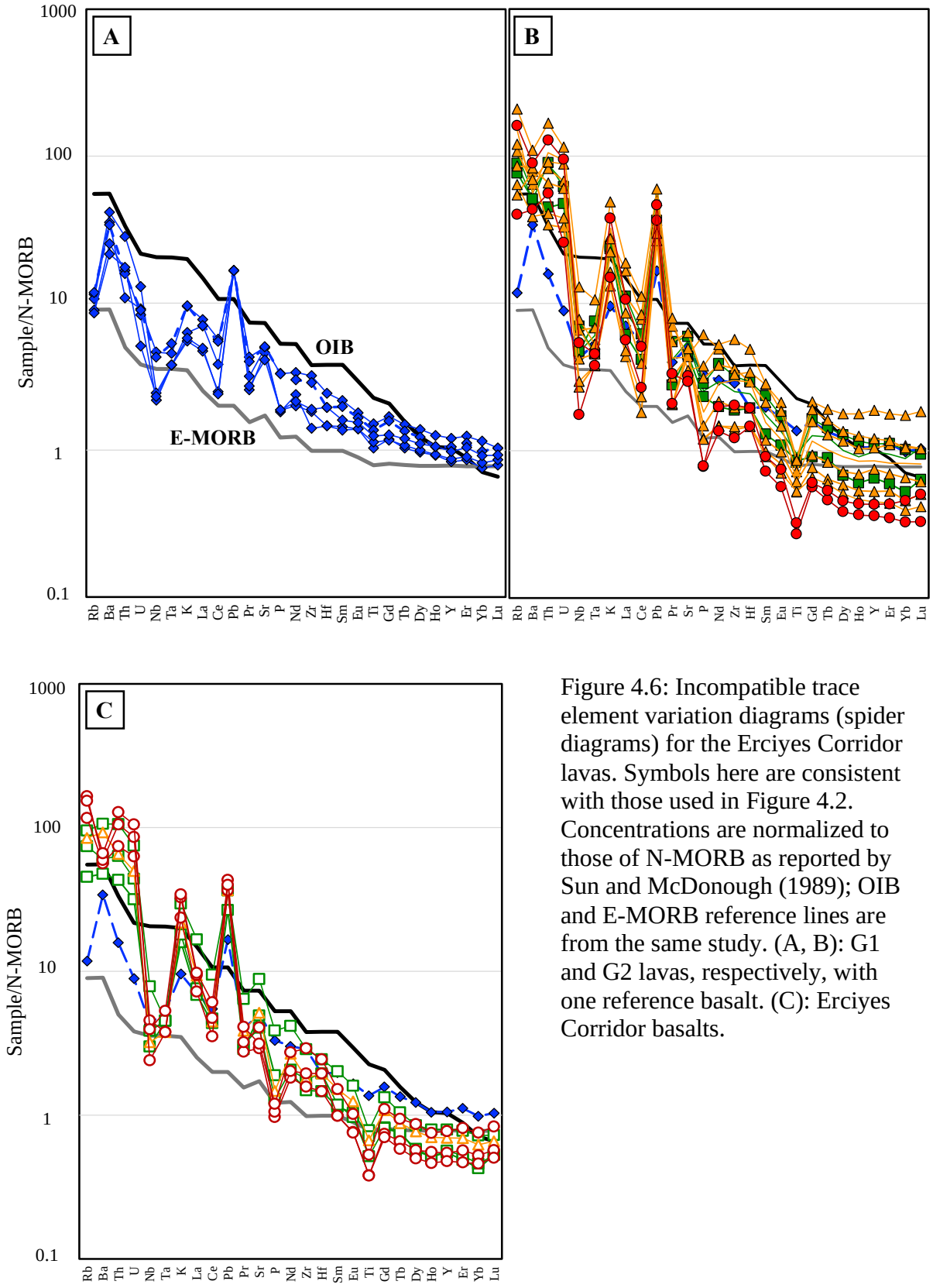

Figure 4.6: Incompatible trace element variation diagrams (spider diagrams) for the Erciyes Corridor lavas. Symbols here are consistent with those used in Figure 4.2. Concentrations are normalized to those of N-MORB as reported by Sun and McDonough (1989); OIB and E-MORB reference lines are from the same study. (A, B): G1 and G2 lavas, respectively, with one reference basalt. (C): Erciyes Corridor basalts.

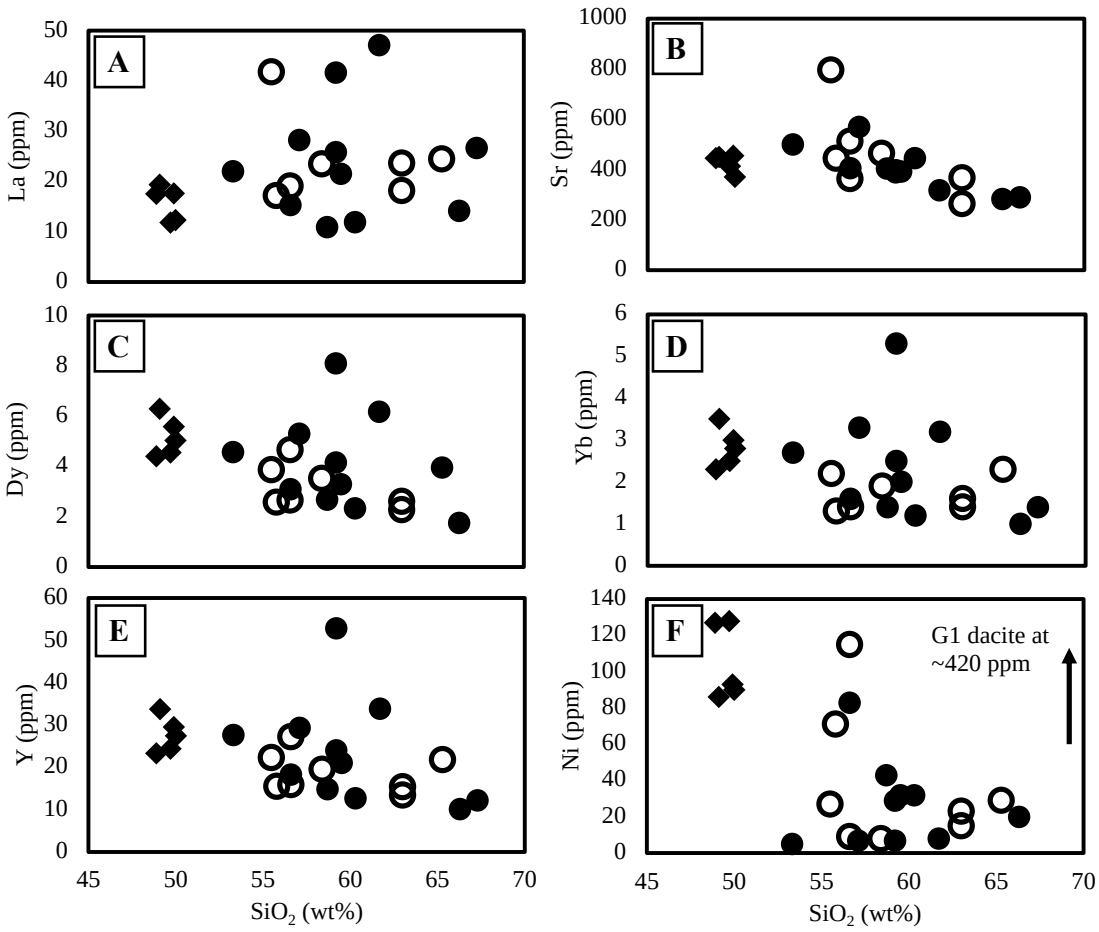

Figure 4.7: Trace element variation diagrams for select elements in the Erciyes Corridor lavas. Symbols are same as those used for Figure 4.3.

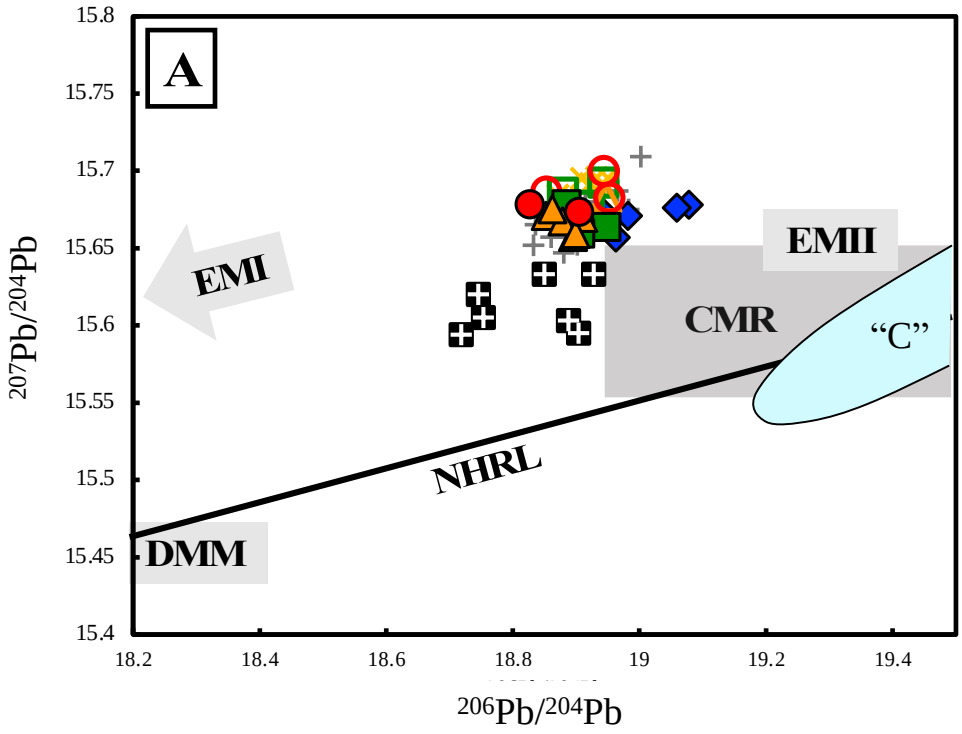
A
EMI
EMII
CMR
"C"
NHRL
DMM
15.8
15.75
15.7
15.65
15.6
15.55
15.5
15.45
15.4
18.2
18.4
18.6
18.8
19
19.2
19.4
207Pb/204Pb
206Pb/204Pb

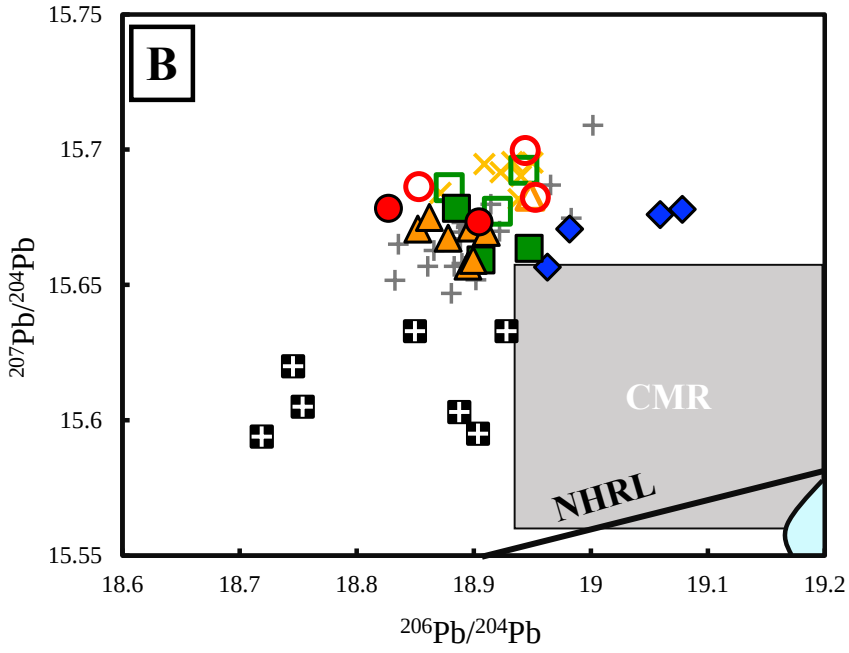
B
CMR
NHRL
15.75
15.7
15.65
15.6
15.55
18.6
18.7
18.8
18.9
19
19.1
19.2
207Pb/204Pb
206Pb/204Pb

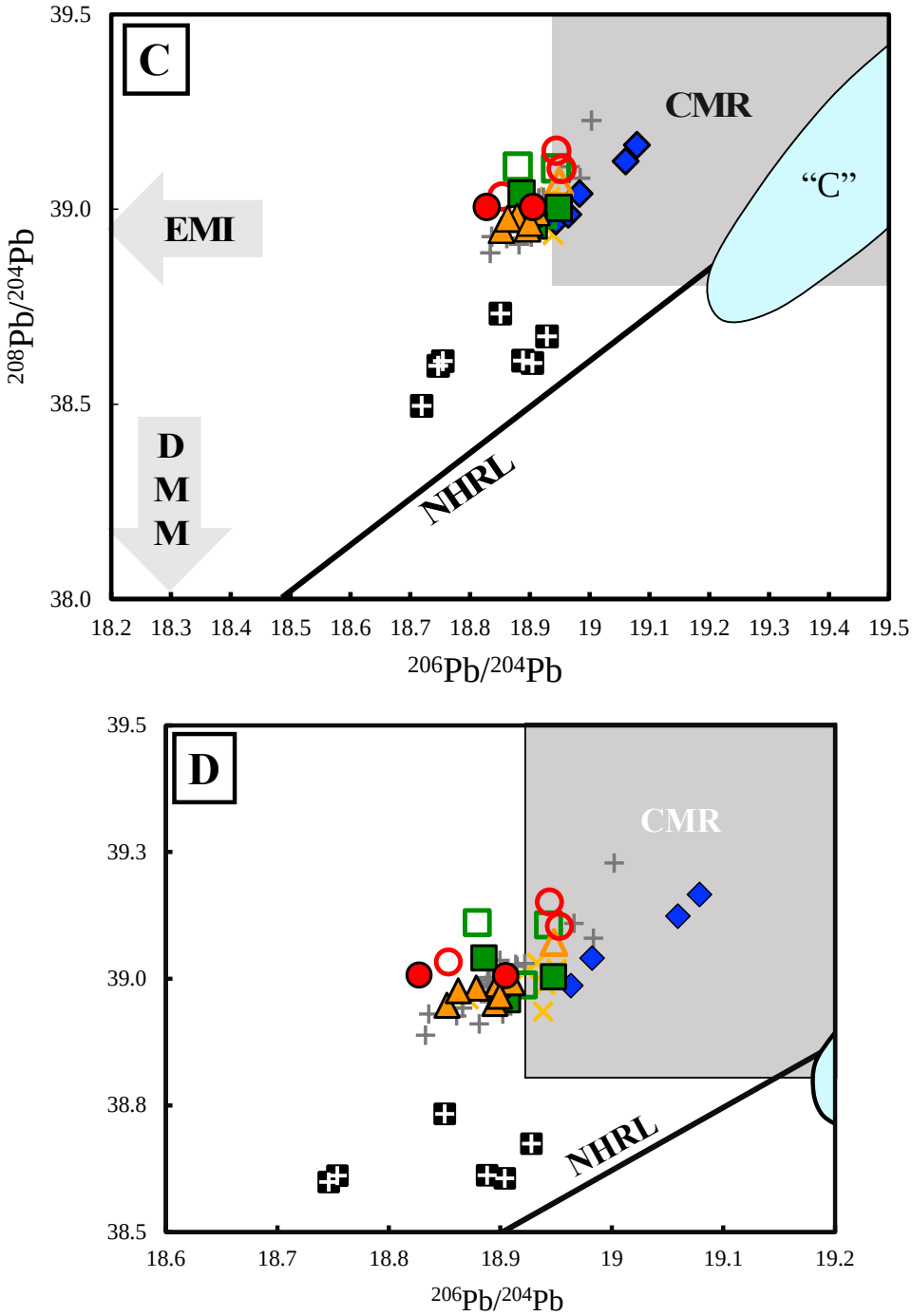

Fig. 4.8: (A and B) $^{207}Pb/^{204}Pb$ vs $^{206}Pb/^{204}Pb$ and (C and D) $^{208}Pb/^{204}Pb$ vs $^{206}Pb/^{204}Pb$ for Erciyes Corridor lavas, shown at different scales. Symbols for Erciyes Corridor lavas, HMC basalts, and Eastern Mediterranean sediments are the same as those used in Figure 4.2. Also included are the Kula basalts from Chakrabarti et al., (2012), represented by black squares with white crosses. General isotopic signatures of mantle reservoirs from Albarede (2009), the Northern Hemisphere Reference Line (NHRL) from Hart (1984), common mantle reservoir for circum-Mediterranean basalts (CMR) from Lustrino and Wilson (2007), and common mantle domain ("C") from Hanan and Graham (1996) are also included for reference.

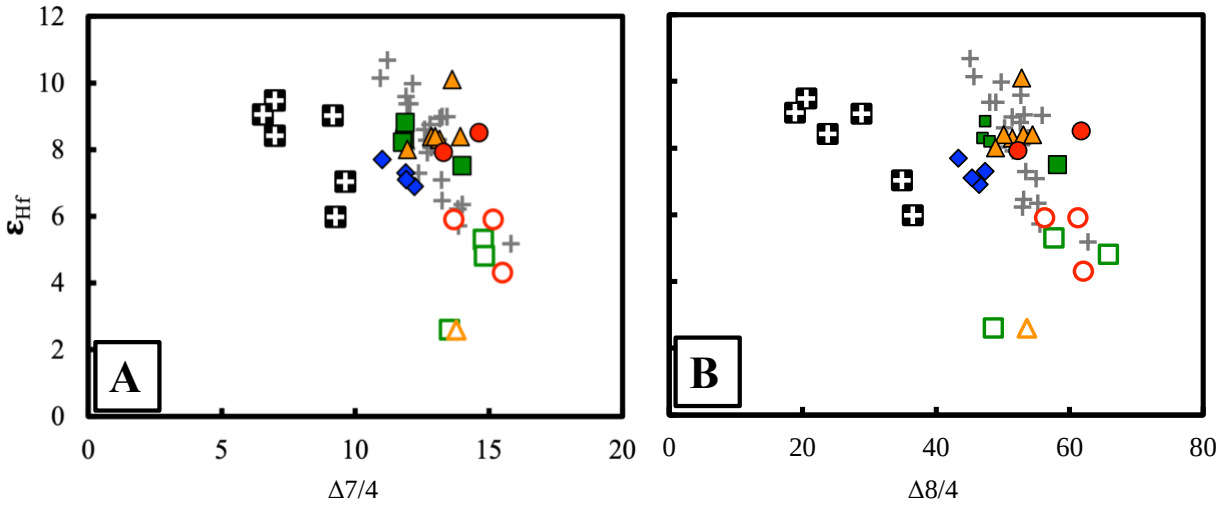

Figure 4.9: εHf vs A) Δ7/4 and B) Δ8/4 for the Erciyes Corridor lavas with the addition of the HMC basalts and Kula basalts. Symbols are same as those in Figures 4.8.

CHAPTER 5: INTERPRETATIONS AND DISCUSSION

Basalts of the Erciyes Corridor are distinctly different from the more evolved lavas in their isotopic composition, in addition to their trace element characteristics. Basalts have higher $^{206}Pb/^{204}Pb$ and range to lower Δ7/4 and Δ8/4 values than those of the evolved lavas. ε_{Hf} values are comparable to those in the G1 lavas, but are higher than those in the G2 lavas. As I will show, these differences cannot be explained via crystal fractionation, which must mean that there are different sources for the basalts and the evolved lavas. For these reasons, the basalts and evolved lavas of the Erciyes Corridor will be discussed separately.

5.1 Two groups of evolved Erciyes Corridor lavas

Evolved lavas of the Erciyes Corridor have similar mineral assemblages, and coherent major element and trace element variations. A key distinction between different Erciyes Corridor evolved lavas is their isotopic compositions. Two distinct trends are apparent in ε_{Hf} when compared against another chemical variable like SiO_2 (Figure 5.1). One group of evolved lavas (designated Group 1 or G1) has nearly invariant ε_{Hf} with increasing silica content, clustering around +8. A second group of evolved lavas (designated Group 2 or G2) has lower, more variable ε_{Hf} values (+2.6 to +5.9; Figure 5.1), ones that are lower than those of most basalts. This group also exhibits a tendency toward higher Pb isotope ratios: median values of Δ7/4 = 14.3 and Δ8/4= 59.5 are close to the upper end of the ranges in G1 lavas (Δ7/4= 11.8 to 14.6 and Δ8/4= 46.9 to 61.8).

Minerals crystallizing from magmas do not detectably incorporate one isotope of the heavier elements over another. Using Hf as an example, the relative mass difference between ^{176}Hf and ^{177}Hf is small and corrections for mass fractionation associated with mass spectrometry usually preclude recognition of mass-dependent variations in $^{176}Hf/^{177}Hf$. For this reason,

variations in ε_{Hf} values require more than one magmatic source. ε_{Hf} values in the G1 lavas are somewhat higher than those of the Erciyes Corridor basalts, but within the range of those for the Hasan Monogenetic Cluster (HMC). The latter are interpreted to be more primitive, having experienced little differentiation since derivation from their mantle source (Reid et al., 2017). The compositional diversity of G1 lavas, despite a narrow range of ε_{Hf}, might therefore be explained by differentiation dominantly via crystal fractionation with negligible crustal contamination. By comparison, the G2 lavas have more variable ε_{Hf} values, intermediate between those of basalts of the HMC and Cappadocian ignimbrites, that generally decrease with increasing SiO_2 (Figure 5.1). The Cappadocian ignimbrites are inferred to have assimilated up to 80% crustal material (Akin et al., 2021). The lower ε_{Hf} of the G2 lavas compared to the G1 lavas may therefore be explained by contributions from crustal contamination. A role for crustal contamination may be further supported by their higher $\Delta 7/4$ and $\Delta 8/4$ values as compared to the G1 lavas.

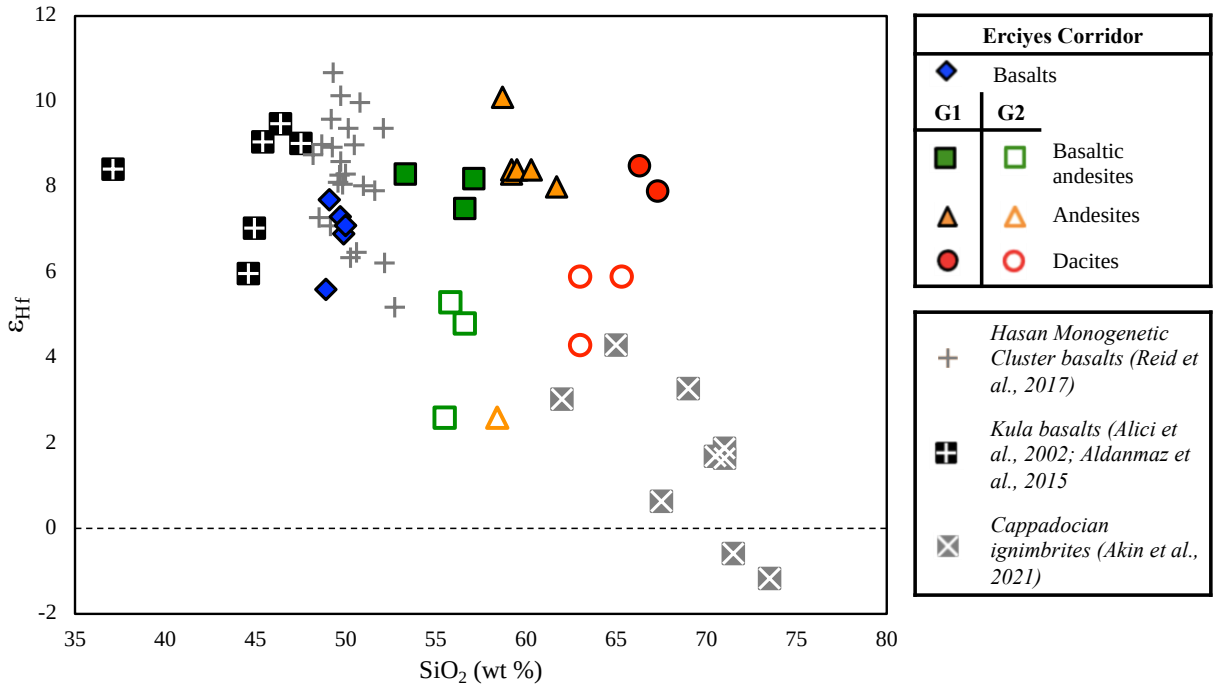

Figure 5.1: ε_{Hf} versus SiO_2 (wt. %) for Erciyes Corridor lavas. Also included are HMC basalts, Kula basalts, and Cappadocian ignimbrites.

5.2 Effects of crystal fractionation in evolved Erciyes Corridor lavas

Crystal fractionation is one mechanism for producing intermediate and silicic magmas from a basaltic parent magma. As a magma body progressively cools, crystallization of minerals occurs in response. Crystallizing minerals remove chemical components from the magma, therefore changing the concentrations of elements in the residual liquid, so long as the crystallized minerals are effectively separated from the liquid. Crystallizing magmas follow a broadly consistent pattern of minerals present based on temperature and magma composition, from higher proportions of mafic minerals to assemblages progressively dominated by more felsic minerals. Understanding this process and how crystallizing minerals can preferentially incorporate different elements can be useful when explaining chemical variations in a suite of lavas.

Based on thin section observations (Chapter 4), Erciyes Corridor evolved lavas contain plagioclase, orthopyroxene, clinopyroxene, hornblende, and opaque oxide minerals. The influence of fractionation of these mineral phases on the lavas' chemical heterogeneity is evident in part in the major element variation diagrams (Figure 4.3). Decreases in MgO with increasing differentiation may be the result of crystallizing clinopyroxene, orthopyroxene, and/or hornblende; decreasing CaO could be the result of fractionation of clinopyroxene, hornblende, and calcic plagioclase. Decreasing FeO is predominantly controlled by crystallization of iron oxides (e.g., magnetite). Decreasing TiO_2 is most likely due to the crystallization of ilmenite, but could also be attributed to titanite fractionation, which will be discussed in more depth below. To examine the effects of crystallizing phases on trace element concentrations, crystal fractionation was modeled for the G1 lavas. This was done only for the G1 evolved lavas, rather than for all evolved lavas, as the variable ε_{Hf} values in the G2 lavas could reflect crustal contamination. As crystal fractionation would not change the isotopic composition of a magma, simple crystal fractionation modeling would therefore not be expected to produce accurate results. Crystal fractionation modeling was done using the Rayleigh equation:

$$C_L = C_O \times F^{D-1}$$

Where C_L= concentration of an element in a residual liquid; C_0= initial concentration of the same element in the melt; F= fraction of liquid remaining; and D= bulk partition coefficient for the crystallizing assemblage.

Partition coefficients reflect an element's affinity for crystallizing phases or, conversely, its tendency to remain in the liquid. Elements with a partition coefficient greater than 1 are considered compatible in a given phase, while elements with partition coefficients less than 1 are considered incompatible. Partition coefficients used in this study are included as Appendix Table 3.

Specific elements were chosen to represent different chemical affinities during crystal fractionation: Sr (LILE), La (LREE), Dy (middle rare earth element, or MREE), Yb (HREE), Y (high field strength element; HREE-like), and Cr and Ni (compatible in mafic minerals). Different proportions of the minerals observed in thin section were modeled, while also allowing for the possible role of common accessory minerals in volcanic rocks. The assumed starting composition was that of a generalized G1 basaltic andesite, based on the median concentrations of each element in the G1 basaltic andesites (n = 3). The target concentration was that of a generalized G1 dacite, constructed similarly from the compositions of G1 dacites (n = 2), with the exception of the more compatible elements Ni and Cr, where minimum G1 dacite values were used. It was determined that trace element variations between the basaltic andesites and dacites of the Erciyes Corridor G1 lavas could be explained by 10% crystallization (F= 0.90) of ~40% plagioclase, ~35% hornblende, ~15% clinopyroxene, and ~10% orthopyroxene (Figure 5.2). It was determined that approximately 5% apatite or 0.5% titanite crystallization in addition to the major mineral phases could help to explain discrepancies in the MREE. Crystallization of these phases in these proportions could not, however, account for highly variable concentrations of Ni and Cr in the G1 evolved lavas. Ni contents range from 5 to 115 ppm in the basaltic andesites (n = 3) and from 20 to 427 ppm in the dacites (n = 2). Chromium contents in the basaltic andesites range from 10 to 209 ppm and from 36 to 111 ppm in the dacites. Both elements are compatible in all crystallizing phases except plagioclase. With the selected partition coefficients and the proposed mineral assemblage, the bulk partition coefficients for Ni and Cr are ~15 and 18, respectively, and therefore progressive crystallization is expected to lower their concentrations rather than to increase them. Thus, the G1 dacite Ni concentration of 427 ppm is

anomalous. For the modeled fractionation of the median G1 basaltic andesites to fit the median G1 dacites, the bulk partition coefficient for each element would need to be closer to ~5.

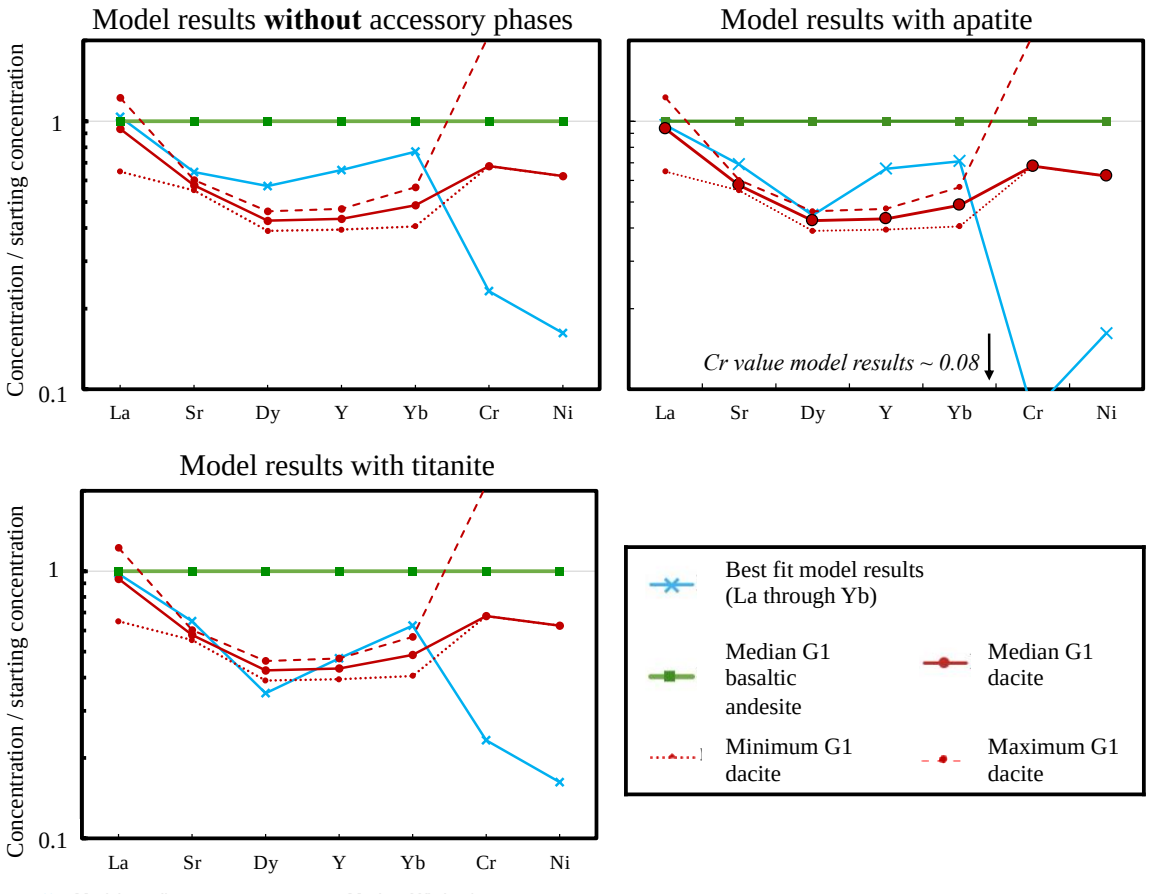

Figure 5.2: Graphical representation of the results of crystal fractionation modeling for select elements. Crystallizing minerals include plagioclase, hornblende, clinopyroxene, and orthopyroxene ± apatite or titanite. Median values refer to the median of all G1 concentrations for each composition (basaltic andesites n = 3, dacites n = 2), except for Ni and Cr concentrations, where the minimum concentrations were used. Median G1 dacite compositions and modeled result values are normalized to the values of the median G1 basaltic andesite (starting) composition. Minimum and maximum G1 dacite compositions are also included for reference.

Considering the phenocrysts observed in thin section, fractionation of plagioclase likely explains the decrease in Sr concentrations between the G1 basaltic andesites and dacites. Plagioclase is the only major mineral in igneous rocks that preferentially incorporates Sr during crystallization (McBirney, 1993). Concentrations of Sr are plotted against La to illustrate the effect of differing degrees of mineral crystallization (Figure 5.3A). While La is incompatible in

other major mineral phases, progressive plagioclase crystallization produces a sharp decrease in Sr concentration. The trend anticipated for plagioclase fractionation can explain the displacement of the G1 Erciyes Corridor dacites and some of the andesites to lower Sr contents from the main trend defined by the basaltic andesites. Therefore, plagioclase fractionation could have occurred after magmas evolved to andesitic compositions. This could be supported by the behavior of Al_2O_3 in the G1 lavas (Figure 4.3). Al_2O_3 concentrations in the Erciyes Corridor basalts and basaltic andesites are constant, and then decrease in concentrations of SiO_2 > 60%, which could indicate plagioclase fractionation. Some of the variability in Sr and La concentrations could, by comparison to heterogeneity in CAVP basalts, also reflect scatter in the concentrations of these elements in the parental melts.

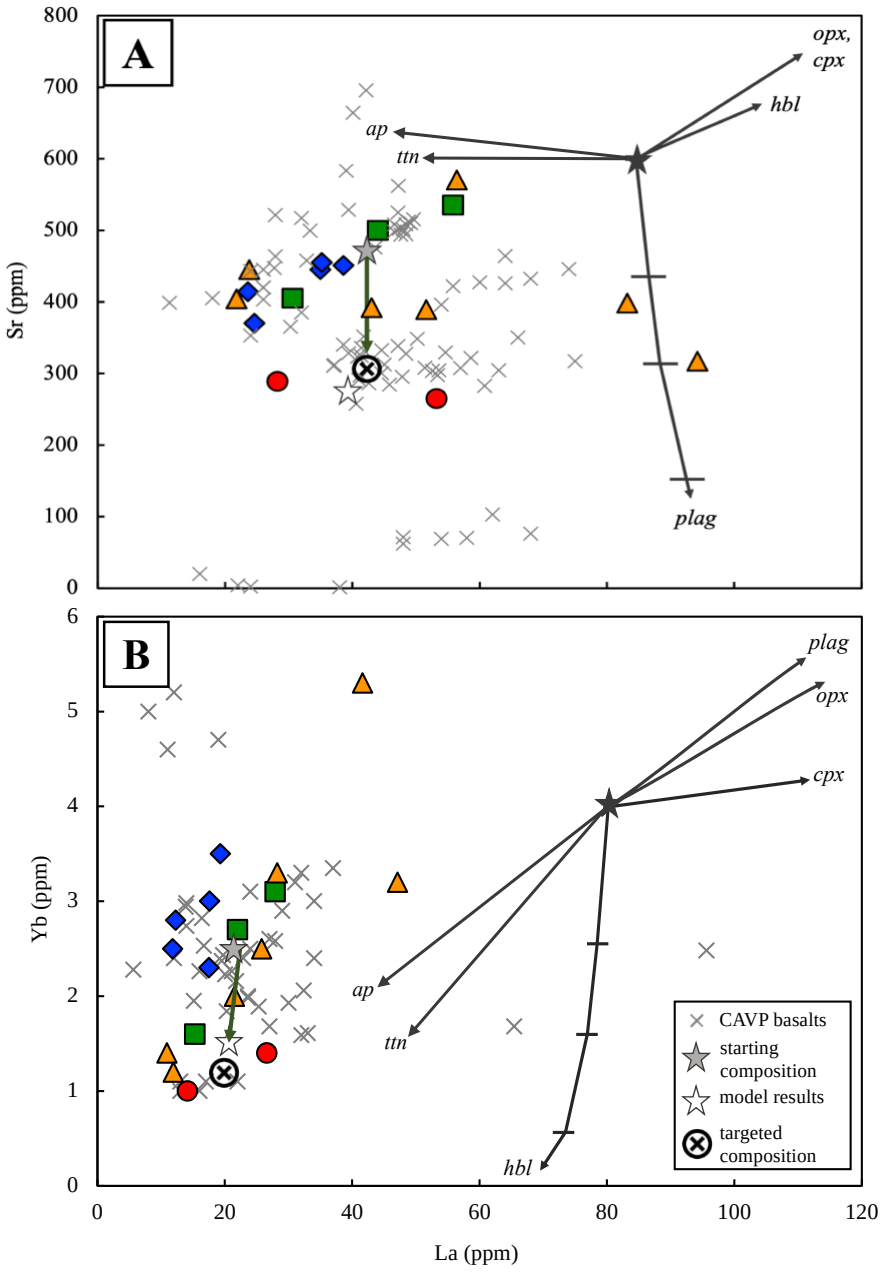

Figure 5.3: A) Sr and B) Yb concentrations (ppm) against La (ppm) for Erciyes Corridor G1 lavas (symbols the same as Figure 5.1). The compositions of other CAVP basalts are also included (gray "x" symbols; from Uslular et al. (2019)). Dark gray vectors show trajectories for fractionation of individual mineral phases. Vectors in (A) represent 30% orthopyroxene (opx), clinopyroxene (cpx), and hornblende (hbl), 5% apatite (ap), 0.5% titanite (ttn), and increments of 5, 10 and 20% plagioclase (plag). Vectors in (B) represent 30% opx, cpx, and plag, 5% ap, 0.5% ttn, and increments of 5, 10, and 20% hbl.

Concentrations of HREE are higher in G1 basaltic andesites than the G1 dacites, which requires removal of HREE during crystallization. Heavy rare earth elements can be compatible in clinopyroxene and orthopyroxene, but only when those phases crystallize in dacitic to rhyolitic lavas (Rollinson, 1993; Appendix Table 2). HREE are more compatible in hornblende than in the pyroxenes, therefore hornblende crystallization will dominate the incorporation of HREE compared to pyroxenes. HREE are notably compatible in garnet, but this mineral is unlikely to be responsible for this discrepancy, as garnet fractionation would increase Dy/Dy*, Dy/Yb, and Ti/Ti* (gray vectors, Figure 4.5) compared to what is seen in the G1 lavas.

While crystallization of an assemblage containing approximately 35% hornblende could potentially explain the overall decrease in HREE concentrations between the G1 basaltic andesites and dacites, the major phases are unable to explain the discrepancies in the MREE. The effect of hornblende crystallization on Dy/Dy* is represented by vectors on Figure 4.5. Hornblende crystallization can partly lower the concentration of MREE in a residual magma, but crystallization of more hornblende than the proportion proposed would mean lowering the proportions of other minerals, such as plagioclase, which would then fail to explain the discrepancies in other elements (such as Sr). For this reason, fractionation of a mineral that can preferentially incorporate MREE over LREE is required to explain lower MREE concentrations in the G1 dacites.

Two common accessory phases which may lower MREE and HREE concentrations in volcanic rocks are apatite and titanite. Neither apatite nor titanite have been identified in thin sections of the evolved Erciyes Corridor lavas, though their absence in thin section does not preclude their crystallization at depth. Apatite is often an accessory phase throughout the volcanic compositional spectrum (Wilson, 1989); titanite is more commonly found in high silica

rocks, though it is still plausible to have titanite fractionation in mafic rocks (Kohn, 2017). Additionally, both phases have been documented in other CAVP lavas (apatite in lavas from the Niğde region (Aydin, 2008); titanite in basaltic andesites from the Tepekoy Volcanic Center (Kuscu and Geneli, 2010)).

Partition coefficients for MREE and HREE in apatite range from ~47 for Dy to 15 in Yb (Rollinson, 1993; Appendix Table 3), meaning that a small amount of apatite fractionation will greatly reduce concentrations of these elements in a melt. As P_2O_5 is a stoichiometric component in apatite, crystallization of apatite will also decrease P_2O_5 concentrations in a suite of lavas. Concentrations of P_2O_5 generally decrease from the G1 basaltic andesites to dacites (Figure 4.3; median P_2O_5 concentrations for G1 basaltic andesites and dacites are 0.30 and 0.092 wt.%, respectively). This change in concentration could be accommodated by fractionation of approximately 0.5 wt.% apatite. Apatite fractionation could then explain increasing paired Th/Yb-Nb/Yb values (Figure 5.5) and decreasing paired Dy/Dy*-Dy/Yb values (Figure 4.5) from G1 basaltic andesites to dacites.

Fractionation of an assemblage of apatite was modeled, using the same select elements as previously discussed. In this scenario, melt proportion remained the same, but the fractionated mineral assemblage contained ~35% plagioclase, ~35% hornblende, ~15% clinopyroxene, ~10% orthopyroxene, and ~5% apatite. Model results for the assemblage containing apatite have La and Dy concentrations which approximate those of the median G1 dacite, whereas model concentrations of Sr, Y, and Yb are elevated from the median G1 dacite composition and concentrations of Cr and Ni are too low.

Titanite fraction was then considered to examine whether it could produce a better fit than apatite fractionation. Partition coefficients for MREE and HREE in titanite are particularly high,

ranging from 935 in Dy to 393 in Yb (Appendix Table 3; Bachmann et al., 2005), meaning that a small amount of crystallizing titanite can drastically decrease MREE and HREE concentrations in a residual liquid. Titanite fractionation will, like the effect of apatite on P_2O_5, reduce TiO_2 in a suite of lavas. The median concentrations of TiO_2 between the G1 basaltic andesites and dacites differ by about 0.7 wt.%. If titanite was the only mineral removing TiO_2 in the G1 lavas, approximately 2.5% of the crystallized assemblage could be titanite. Therefore, the estimated removal of 0.5% titanite is permissible so long as another mineral, such as ilmenite, removed the rest of the difference in TiO_2. If titanite crystallization occurred in the Erciyes Corridor G1 lavas, it could explain the chemical variations of the endmembers of the G1 lavas, though the concentrations of both major and trace elements in the andesitic lavas are highly variable. Trends formed by most G1 basaltic andesites through dacites on Dy/Dy*-Dy/Yb, Nb/U-Th/Yb, and Th/Yb-Nb/Yb graphs generally parallel vectors representative of titanite fractionation (Figures 4.5A, 5.4, and 5.5), though the specific values in the andesites are not as well explained by this model.

Titanite fractionation was modeled using an assemblage of 39.5% plagioclase, 35% hornblende, 15% clinopyroxene, 10% orthopyroxene, and 0.5% titanite (Figure 5.2; F = 0.90). In this model, concentrations of La and Y are nearly identical to the median G1 composition, Sr and Yb concentrations are only slightly elevated, and Dy concentrations are slightly too low. As was the case in both previously discussed modeling results, concentrations of compatible elements Ni and Cr are significantly lower than in the G1 dacites. These results suggest the titanite fractionation model better explains the trace element concentrations as compared to the apatite fractionation model.

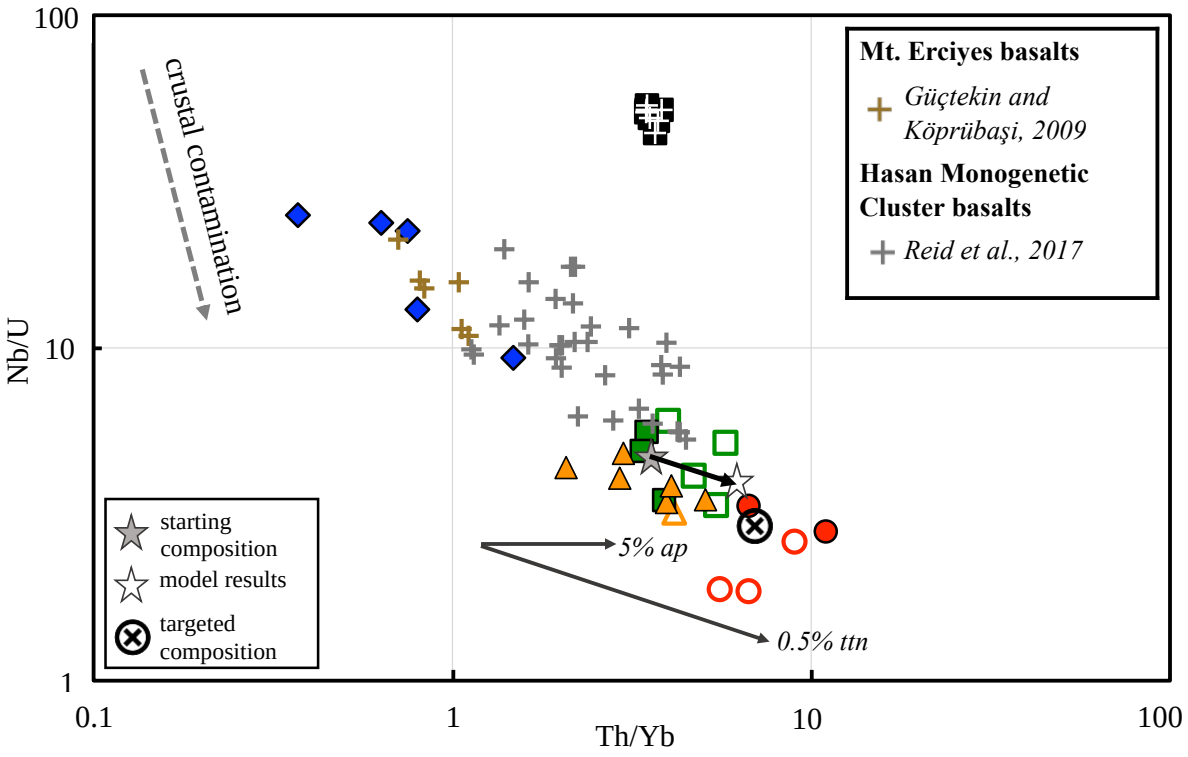

Figure 5.4: Paired Nb/U-Th/Yb for the Erciyes Corridor lavas. Erciyes Corridor lava symbols are the same as those used in Figure 5.1. Also included are Kula basalts (black boxes with white crosses; Aldanmaz et al., 2015). Thin gray vectors represent the effect of 0.5% titanite and 5% apatite fractionation. Thick, dashed gray vector represents the approximate trajectory of crustal contamination.

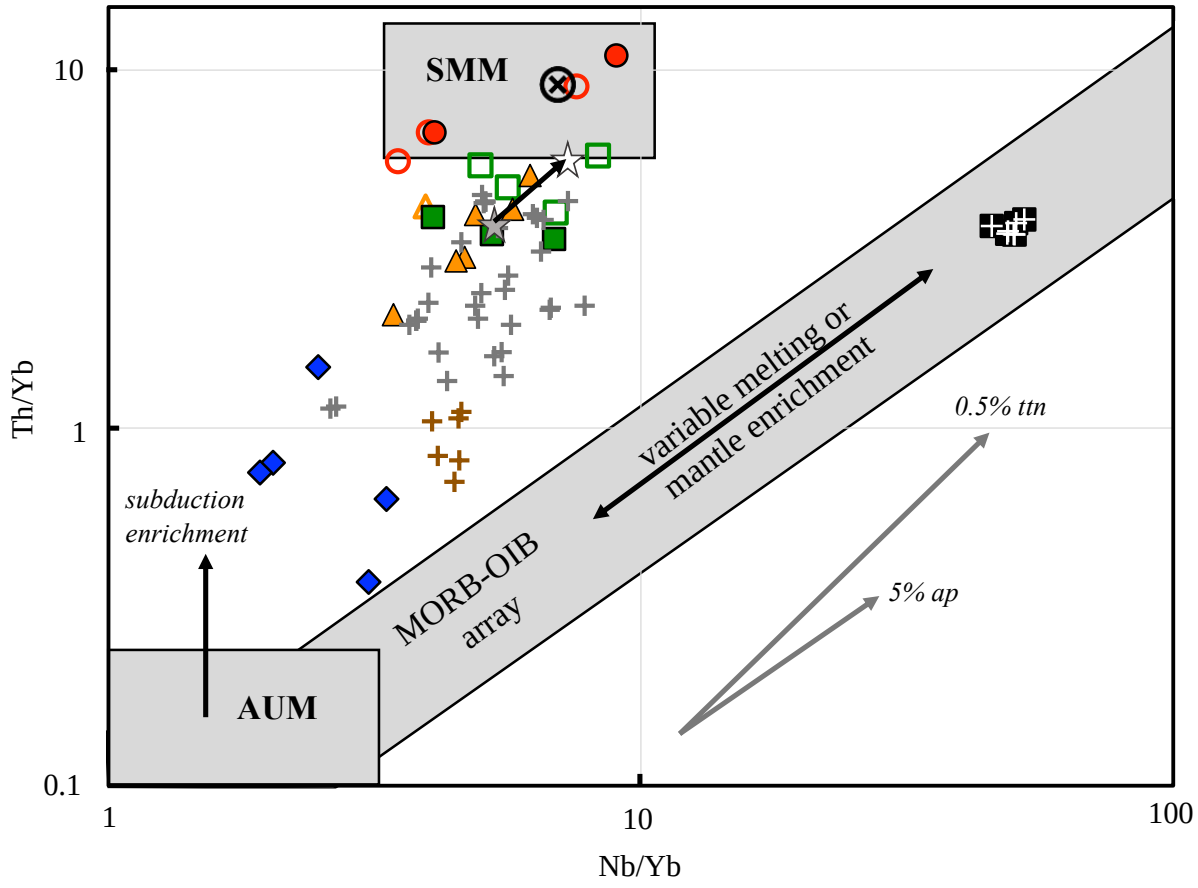

Figure 5.5: Paired Th/Yb-Nb-Yb ratios for the Erciyes Corridor lavas, compared to their distribution in the MORB-OIB array after Pearce et al. (2008). Symbols are the same with those used in Figure 5.5. Gray vectors represent 5% apatite fractionation 0.5% titanite fractionation (partition coefficients included in Appendix Table 3). Model results included here are for the titanite-bearing mineral assemblage.

As titanite is a less common phase than apatite in mafic to intermediate lavas, simulations were run using PhasePlot, a Macintosh-supported software based on MELTS (Ghiorso, 2012), to see if this could provide further support for titanite fractionation. Phase assemblages for the three G1 basaltic andesites were characterized over a temperature range of ~1200 to 600 °C, a pressure range of 300 to 100 MPa, and a water content range of 0 to 5 percent. In these simulations, titanite (sphene) was a predicted phase, but only at low temperatures (< 700 °C) and low pressures (< 200 MPa) with very low percent liquid remaining (< 1%; Figure 5.6). Liquids in

such a near-solidus state would be highly evolved in nature and likely difficult to separate from crystals. It is possible, however, that MELTS-based modeling is not able to accurately reproduce the conditions for titanite saturation, given the uncertainties associated with modeling hornblende-bearing crystal assemblages like those of the Erciyes Corridor G1 lavas (Gualda et al., 2019). The lack of titanite in the model results can therefore be considered inconclusive.

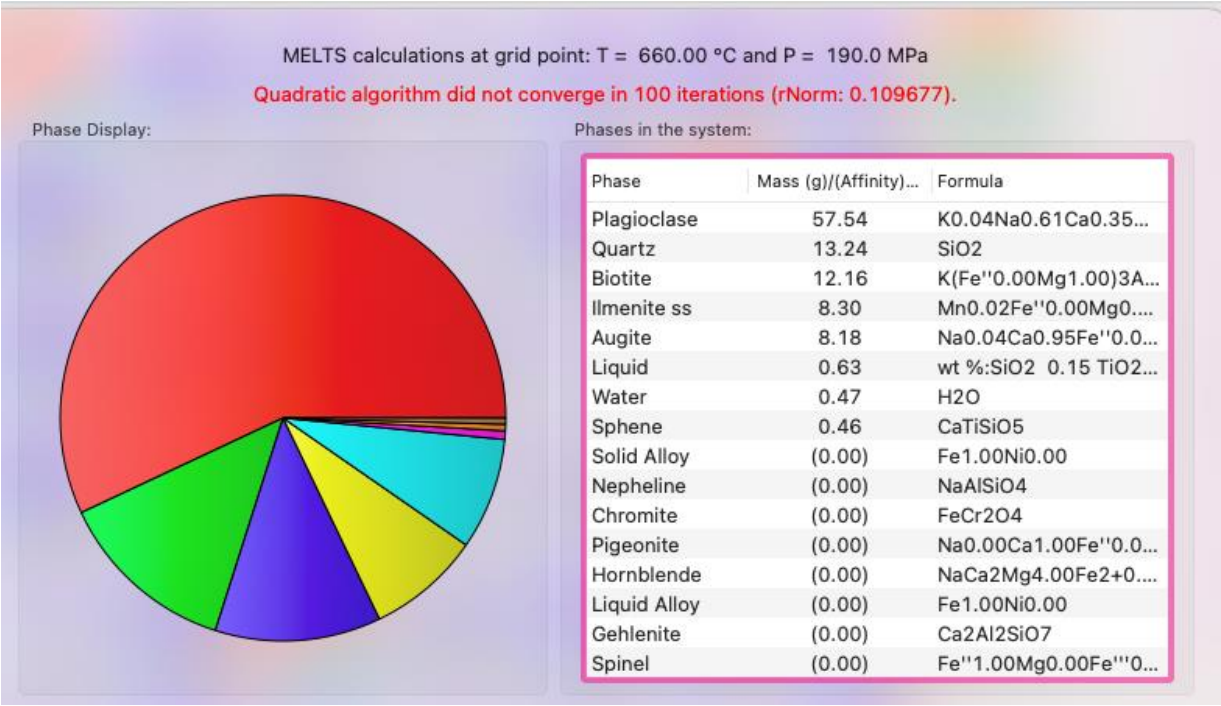

Phase	Mass (g)/(Affinity)...	Formula
Plagioclase	57.54	K0.04Na0.61Ca0.35...
Quartz	13.24	SiO2
Biotite	12.16	K(Fe''0.00Mg1.00)3A...
Ilmenite ss	8.30	Mn0.02Fe''0.00Mg0....
Augite	8.18	Na0.04Ca0.95Fe''0.0...
Liquid	0.63	wt %:SiO2 0.15 TiO2...
Water	0.47	H2O
Sphene	0.46	CaTiSiO5
Solid Alloy	(0.00)	Fe1.00Ni0.00
Nepheline	(0.00)	NaAlSiO4
Chromite	(0.00)	FeCr2O4
Pigeonite	(0.00)	Na0.00Ca1.00Fe''0.0...
Hornblende	(0.00)	NaCa2Mg4.00Fe2+0....
Liquid Alloy	(0.00)	Fe1.00Ni0.00
Gehlenite	(0.00)	Ca2Al2SiO7
Spinel	(0.00)	Fe''1.00Mg0.00Fe'''0...

Figure 5.6: Example of results for evolution of a CAVP basaltic andesite generated using PhasePlot (Ghiorso, 2012). The composition of sample CAT15-KS49, a G1 basaltic andesite was used for this simulation with the addition of 3 wt. % water. An equilibrium phase assemblage, their mass distributions (out of 100 g), and mineral formulas are shown at a temperature of 630 °C and a pressure of 190 MPa. The legend for the colors is not visible in this view but the pie chart segments shown correspond to mineral abundances.

In summary, a mineral assemblage containing trace amounts of apatite or titanite could explain the overall differences between incompatible trace element concentrations of the G1 endmembers (basaltic andesite to dacite). Additionally, a decrease in P_2O_5 and TiO_2 concentrations between these endmembers could be partly explained by apatite or titanite

crystallization, respectively. The scattered characteristics of a subset of the G1 andesites compared to the basaltic andesites may be explained by fractionation of variable mineral proportions or by heterogeneity in parent melts (e.g., CAVP basalts, shown in Figures 5.3A and B).

5.3 Alternative source for G1 lavas: modeling using a primitive CAVP basalt

Evolved G1 lavas were compared to basalts from the Hasan Monogenetic Cluster (HMC; Reid et al., 2017) to determine whether they may have been sourced from a comparable mafic melt. The HMC basalts were used for comparison here, as they are primitive melts (Mg# > 60) and have the full suite of trace element data available. Comparisons were made using three basalts that represent the range of Mg# in the suite, as well as the median value (Figure 5.7).

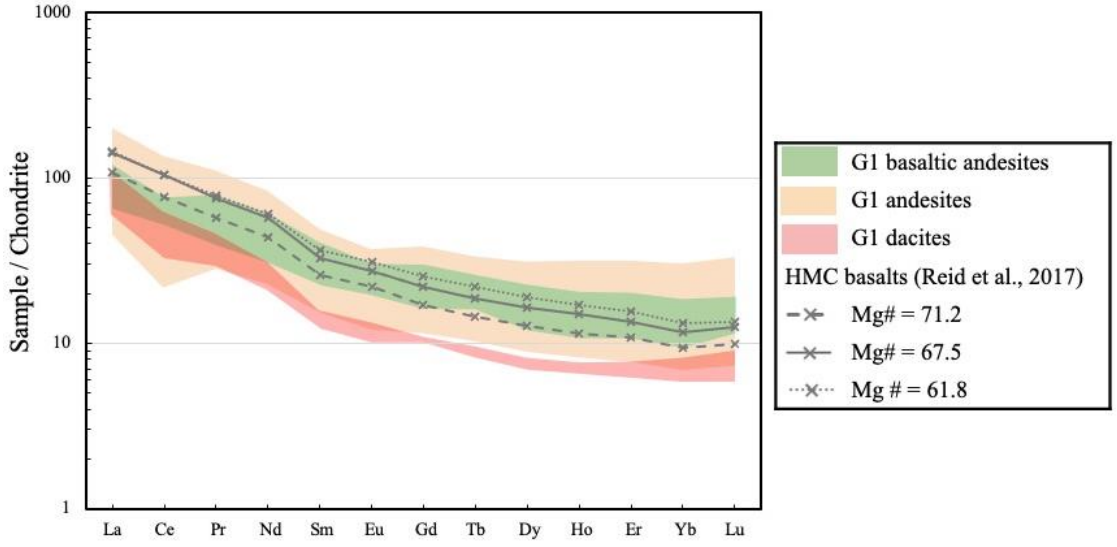

Figure 5.7**:** Rare earth element diagram for Erciyes Corridor G1 lavas compared to basalts from the Hasan Monogenetic Center by Reid et al. (2017). Shaded fields for the Erciyes Corridor lavas encompass the range of concentrations from each lava type.

Unlike Erciyes Corridor basalts, the REE patterns of the HMC basalts to not cross those of the G1 Erciyes Corridor lavas. Chondrite-normalized REE values in the HMC basalts are comparable to those of the G1 basaltic andesites, and intermediate to the wide range of

compositions represented by the G1 andesites. REE concentrations in the G1 dacites are overall lower than in the HMC basalts; crystallization of phases which preferentially incorporate REE, particularly MREE, would therefore still be required to explain the trace element signatures of the G1 dacites.

Fractionation of the G1 lavas using the most primitive basalt from the HMC as the starting composition was modeled (Figure 5.8). It was determined that 15% crystallization of an assemblage containing ~50% plagioclase, ~25% hornblende, ~15% clinopyroxene, and ~10% orthopyroxene would approach the composition of the median G1 dacites. This model is a better overall fit for the MREE and HREE, as well as compatible elements, even though Sr and La are not as well explained. This could mean that the most evolved G1 lavas were derived from basalts similar in composition to those from the HMC rather than from more mafic Erciyes Corridor lavas via fractionation of a mineral assemblage dependent on accessory phases.

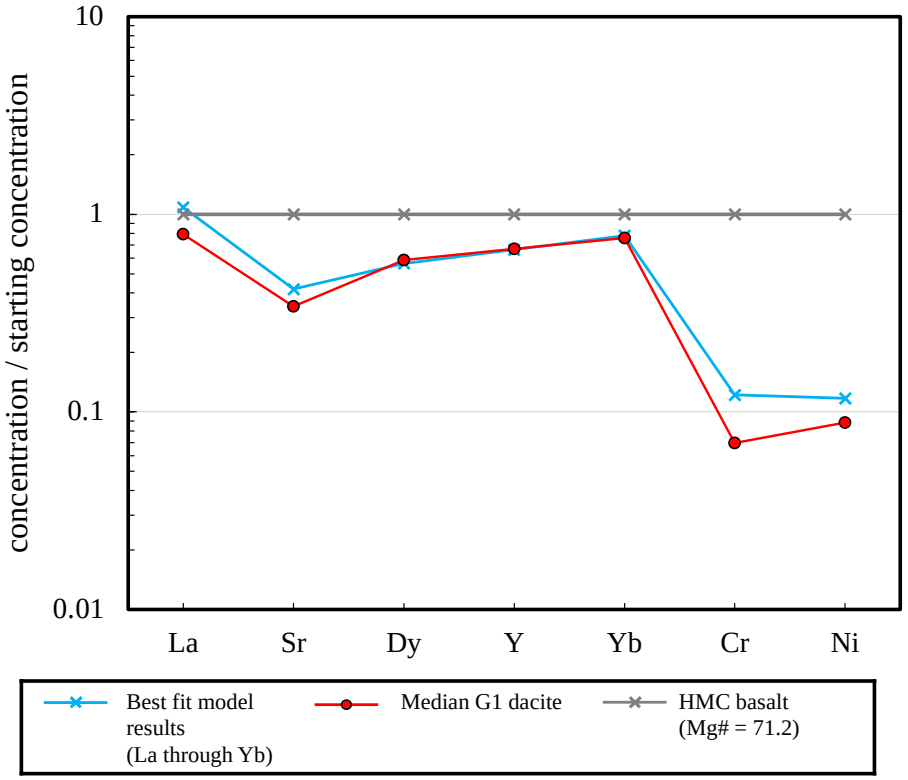

Figure 5.8: Graphical representation of the results of crystal fractionation modeling for select elements. Crystallizing minerals include plagioclase, hornblende, clinopyroxene, and orthopyroxene. Median values refer to the median of all G1 dacite concentrations (n = 2), except for Ni and Cr concentrations, where the minimum concentrations were used. Median G1 dacite compositions and modeled result values are normalized to the values of the most primitive HMC basalt.

5.4 Effects of crustal contamination in evolved G2 Erciyes Corridor lavas

Magmas can differentiate through crystal fractionation alone, but assimilation of wall rock must also be considered. The Hf isotopic compositions of Cappadocian ignimbrites, based on analysis of zircon (Akin et al., 2021), can provide insights into whether crustal contamination has occurred in the Erciyes Corridor evolved lavas. Akin et al. (2021) state that because $^{176}Lu/^{177}Hf$ ratios in zircon crystals of the Cappadocian ignimbrites show negligible radiogenic Hf enrichment post-crystallization, their compositions are reflective of their original source material. As the Cappadocian ignimbrites have been interpreted to have assimilated up to ~80%

crust during their differentiation (Akin et al., 2021), their ε_{Hf} could delimit the effects of crustal contamination on Central Anatolian magmas.

As previously indicated, whereas the G1 evolved lavas are characterized by invariant ε_{Hf} values (~+8), ε_{Hf} values in the G2 lavas are variable, extending to lower values (+2.6 to +5.9). Notably, ε_{Hf} decreases with increasing SiO_2 (Figure 5.1). The G2 lavas also have higher $\Delta 7/4$ and $\Delta 8/4$ values than the G1 lavas, despite their similar $^{206}Pb/^{204}Pb$. Crustal values of ε_{Hf} are anticipated to be lower than the ε_{Hf} values of the mantle (e.g., White, 2013), a difference that is reflected by the isotopic contrast between primitive HMC basalts and the crustally dominated Cappadocian ignimbrites in ε_{Hf} -SiO_2 space (Figure 5.1). The G2 Erciyes Corridor lavas are intermediate to the HMC basalts and the Cappadocian ignimbrites in this respect, which suggests that the G2 lavas could reflect increasing amounts of crustal contamination with increasing differentiation. Although Pb isotope data are not available for the Cappadocian ignimbrites for direct comparisons, the elevated $\Delta 7/4$ and $\Delta 8/4$ of the G2 lavas with respect to the G1 lavas may also be a product of crustal assimilation.

Paired ratios of Nb/U and Th/Yb can be useful for investigating whether crustal contamination occurred (Figure 5.4). Ratios of Nb/U are fairly constant in mantle sources (Hoffman et al., 1986), whereas crustal values of Nb/U are markedly lower (Rudnick and Gao, 2013). Increasing Th/Yb can indicate either subduction enrichment or crustal contamination (Pearce et al., 2008; Dogan et al., 2013). If crustal contamination occurred, Nb/U should decrease with increasing Th/Yb. Titanite fractionation is also expected to have a similar effect, affecting Th/Yb values more than Nb/U values (represented by a gray vector on Figure 5.4). Nb/U values decrease more sharply with increasing Th/Yb in the G2 evolved lavas than in the

G1 evolved lavas, a pattern that is attributed here to crustal contamination, with or without titanite fractionation.

5.5 Erciyes Corridor basalts and their sources

As described in Chapter 4, the Erciyes Corridor basalts have notably different trace element and isotopic characteristics compared to the evolved lavas (e.g., less steep REE patterns, higher $^{206}Pb/^{204}Pb$, lower $\Delta 7/4$, $\Delta 8/4$ in some basalts). For this reason, it is useful to consider the Erciyes Corridor basalts in comparison to other CAVP basalts, with the main foci for comparison being basaltic lavas from Mt. Erciyes and the HMC. Mt. Erciyes basalts, erupted in the same general region as the Erciyes Corridor lavas but in the Quaternary Period, represent a temporal contrast to the Miocene- to Pliocene Erciyes Corridor lavas. The HMC basalts provide both a temporal and geographical contrast given that they erupted during the Quaternary Period in a location toward the southwest extent of the CAVP. These comparisons will be used to interpret potential sources for the Erciyes Corridor basalts.

Basalts of the Erciyes Corridor are calc-alkaline to weakly alkaline (Figure 4.2A), as are the basalts of Mt. Erciyes and the HMC. The Erciyes Corridor basalts generally have LILE and LREE concentrations that are intermediate to lower than those from Mt. Erciyes and the HMC basalts (Figure 5.9). MREE and HREE concentrations in the Erciyes Corridor basalts overlap concentrations of those elements in Mt. Erciyes basalts and the intermediate to upper range of those elements in the HMC basalts. HFSE concentrations in these lavas are highly variable; Ti concentrations in the Erciyes Corridor basalts are intermediate to those in the Mt. Erciyes and HMC basalts, and Nb and Ta contents are similar to the middle to lower range of the HMC basalts.

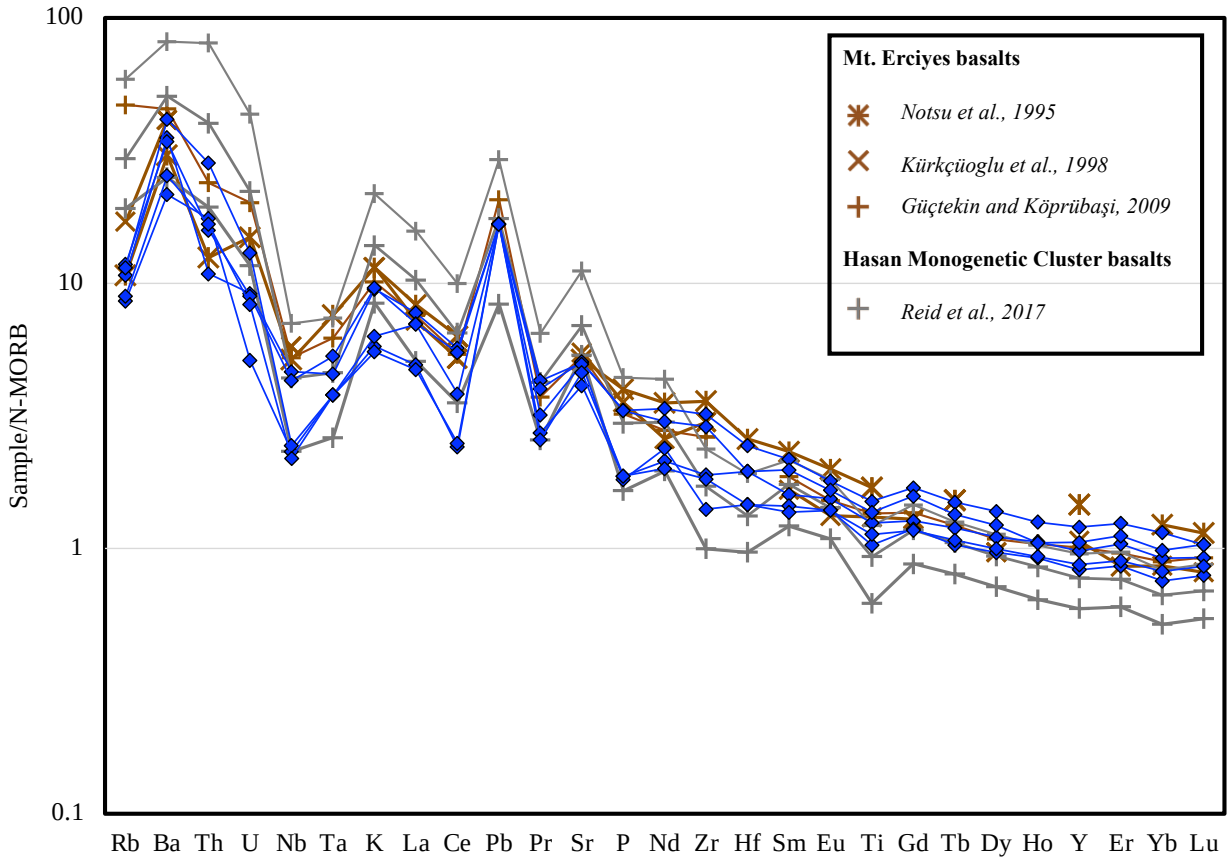

Figure 5.9: Incompatible trace element diagram comparing the Erciyes Corridor basalts to basalts from Mt. Erciyes and the HMC. Values are normalized to N-MORB using values from Sun and McDonough, 1989. Mt. Erciyes basalts represent median values from their respective studies (n = 3 for each study) whereas the maximum, minimum, and median values for the HMC (n = 33) are included.

Paired ratios between nominally incompatible trace elements provide better resolution of comparisons between these lava suites and determinations of their likely source contributions. The Erciyes Corridor basalts are contained within the MORB field in both Dy/Dy*-Dy/Yb and Dy/Dy*-Ti/Ti* space (Figure 4.5). Dy/Dy*-Ti/Ti* values in the Erciyes Corridor basalts also overlap with the field defined by circum-Mediterranean anorogenic basalts (CiMACI; Lustrino and Wilson, 2007) and the AUM (ambient upper mantle) component delimited by Reid et al. (2017).

Whereas the Mt. Ericyes, and HMC basalt groups also overlap with the MORB field in Dy/Dy*-Dy/Yb space, values in the Erciyes Corridor basalts are more tightly clustered compared to those of the other suites. The HMC lavas extend to lower Dy/Dy* and higher Dy/Yb values than either the Erciyes Corridor basalts or the Mt. Erciyes basalts, approaching the composition of the Kula basalts (Chakrabarti et al., 2012). In Dy/Dy*-Ti/Ti* space, the Erciyes Corridor basalts mostly overlap with the generalized characteristics of the AUM component delimited by Reid et al. (2017). The Mt. Erciyes basalts extend to lower Dy/Dy* and higher Ti/Ti* values compared to the Erciyes Corridor basalts, approaching the composition of OIB (Sun and McDonough, 1989). Conversely, the HMC basalts extend to lower Dy/Dy* and Ti/Ti* towards the SMM field delimited by Reid et al. (2017).

Paired Th/Yb-Nb/Yb ratios after Pearce et al. (2005) were also examined for the basaltic lavas (Figure 5.5). The region defined by the MORB-OIB array can signal the complementary effects of variable melting and/or mantle enrichment, with lavas from the more depleted sources having low paired Th/Yb-Nb/Yb. Elevated Th/Yb at a given Nb/Yb value can be interpreted as subduction enrichment. The Erciyes Corridor basalts have lower Nb/Yb values compared to the majority of the HMC and Mt. Erciyes basalts and are notably displaced towards the more depleted end of the MORB-OIB array and the AUM (Reid et al., 2017). Th/Yb and Nb/Yb values broadly increase from the Erciyes Corridor basalts to the Mt. Erciyes basalts to the HMC basalts. The lower Nb/Yb and Th/Yb ratios of the Erciyes Corridor basalts may reflect derivation from a more depleted, predominantly AUM source, one that is distinct from that responsible for the HMC and Mt. Erciyes basalts. Variable Th/Yb in the Erciyes Corridor basalts suggests some degree of source enrichment by contributions from prior subduction.

In addition to lower Th/Yb values, the Nb/U ratios of the Erciyes Corridor basalts extend to higher values than the majority of the HMC basalts; the Mt. Erciyes basalts are contained within the range of the Erciyes Corridor lavas (Figure 5.4). Decreasing Nb/U can be attributed to crustal contamination, or to the incorporation of the SMM component in this case. The heterogeneity in Nb/U paired with that of Th/Yb may reflect the variable contributions of both AUM and SMM mantle components in the HMC basalts in particular. Higher Nb/U values in the Erciyes Corridor basalts compared to the HMC and Mt. Erciyes basalts therefore support the interpretations gained from the paired Th/Yb-Nb/Yb and Dy/Dy*-Ti/Ti* ratios that the SMM component is less prevalent in the Erciyes Corridor mantle source.

Paired Ce/Y-Zr/Nb ratios, like paired Th/Yb-Nb/Yb ratios, can be used to gauge the relative depletion or enrichment of a mantle source component, with magmas derived from more enriched sources having higher Ce/Y and lower Zr/Nb, and those from depleted sources having lower Ce/Y and higher Zr/Nb; variations in melt fractions could have a compounding effect. The overall lower Ce/Y and higher Zr/Nb values in the Erciyes Corridor basalts compared to the Mt. Erciyes and HMC basalts (Figure 5.10) again could reflect the dominant contribution from the AUM component. Ce/Y and Zr/Nb values additionally may help illuminate the incorporation (or lack thereof) of the OIB-like intraplate component (IPC) in CAVP basalts. Both the HMC and Mt. Erciyes basalts have been interpreted to have had some contribution from an IPC (Kürküoglu et al., 1998; Reid et al., 2017) akin to the source of the Kula basalts of Western Anatolia (Chakrabarti et al, 2012). Although the higher overall Ce/Y and lower Zr/Nb in the HMC and Mt. Erciyes basalts may not be solely from the incorporation of an OIB-like IPC, the overlap in Dy/Dy*-Dy/Yb space between HMC and Kula basalts (Figure 4.5A) and the increase in Ti/Ti* with decreasing Dy/Dy* towards OIB compositions in the Mt. Erciyes basalts (Figure 4.5B)

support the hypothesis that IPC was involved in these lavas. Conversely, the lower Ce/Y and higher Zr/Nb of the Erciyes Corridor basalts suggest that an IPC contributed negligibly to the Erciyes Corridor basalts, as does the lack of deviation from the array between SMM and AUM towards IPC in Th/Yb-Nb/Yb and Dy/Dy*-Ti/Ti* space.

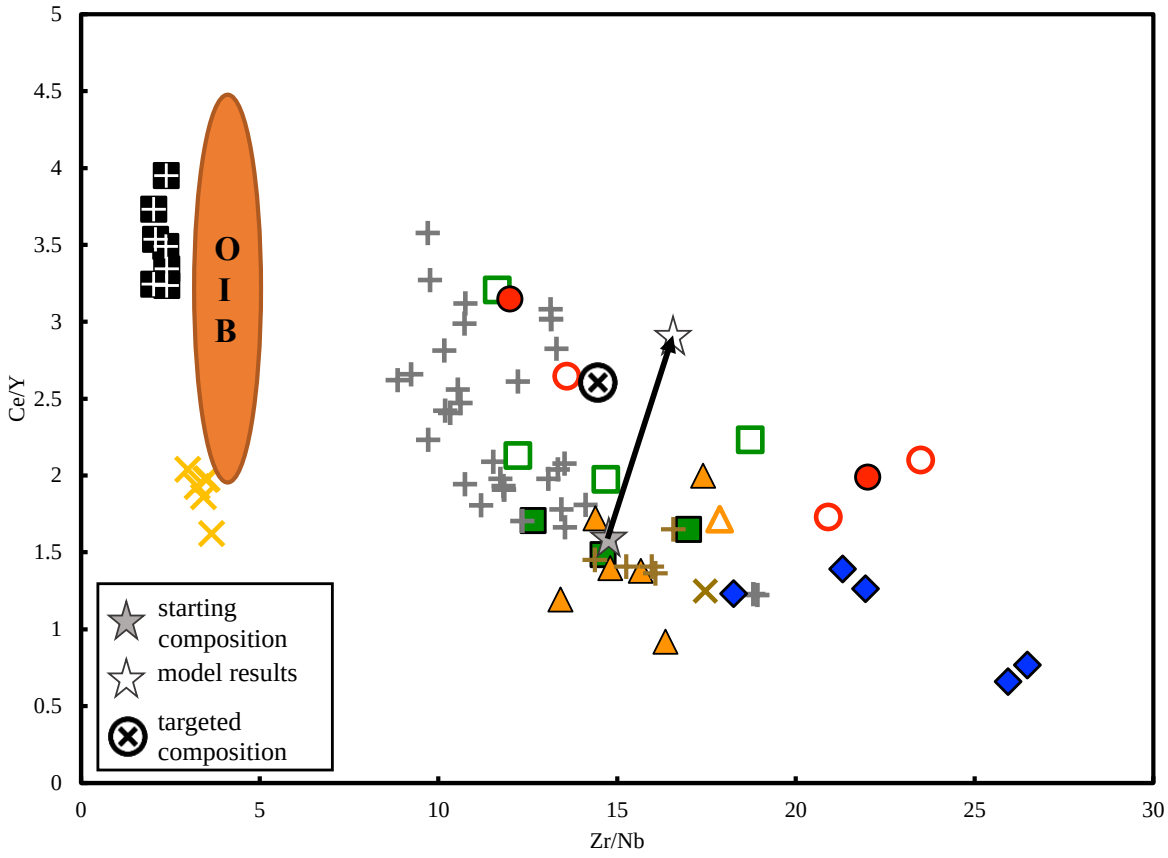

Figure 5.10 Paired Ce/Y-Zr/Nb for the Erciyes Corridor lavas. Symbols for Erciyes Corridor lavas are same as in Figure 5.1. Also shown are HMC and Mt. Erciyes lavas; symbols as in Figure 5.7. Also included are Kula basalts (black boxes with white crosses) from Aldanmaz et al. (2015), proximal Eastern Mediterranean pelagic sediments (yellow x's) from Klaver et al. (2015), and the OIB field as outlined in Kürkcüoglu et al. (1998). Model results included here are for the titanite-bearing assemblage.

In summary, the Erciyes Corridor basalts appear to predominantly reflect melting of the Central Anatolian AUM component (characterized by low paired Th/Yb-Nb/Yb and high Nb/U, and by overlapping signatures in Dy/Dy*-Ti/Ti* space), in contrast to the variable contributions

from AUM, SMM, and to a lesser extent, IPC exhibited by the Mt. Erciyes and HMC basalts. Incorporation of an OIB-like IPC, which may explain certain characteristics of the HMC and Mt. Erciyes basalts (e.g., high Ce/Y and low Zr/Nb), is not required to explain the chemistry of the Erciyes Corridor lavas.

5.6 G1 lavas as additional windows into mantle sources

Examining the influence of different mantle source components on magmatic activity in a particular region is typically conducted on primary melts from the mantle, i.e., basalts. As discussed above, the evolved nature of G1 lavas could be the result of differentiation without appreciable crustal contamination, in which case they may still retain geochemical signatures indicative of their mantle source. The G1 evolved lavas have lower Nb/U and higher Th/Yb compared to the Erciyes Corridor basalts (Figure 5.5), which could be caused by greater incorporation of the SMM component in their parental melts. Titanite fractionation could explain the higher Th/Yb of the more evolved G1 lavas within the suite (Section 5.2) but this is unlikely to account for the higher Th/Yb of the basaltic andesites compared to the basalts. A greater contribution from the SMM to the G1 lavas is supported by the distribution of lavas in Dy/Dy*-Dy/Yb and Dy/Dy*-Ti/Ti* spaces (Figure 4.5), where the G1 lavas extend from signatures of the AUM towards those of the SMM; deviations from the SMM-AUM array in Dy/Dy*-Ti/Ti* space are likely due to hornblende ± titanite fractionation. The dissimilarity of paired ratios such as Dy/Dy*-Ti/Ti* and Nb/U-Th/Yb to those of OIB and OIB-like lavas such as the Kula basalts suggests that the elevated Ce/Y and lower Zr/Nb of the G1 evolved lavas compared to the Erciyes Corridor basalts were more likely the result of greater SMM incorporation rather than incorporation of the IPC. Thus, whereas the Erciyes Corridor basalts likely reflect derivation

dominantly from the AUM, the evolved Erciyes Corridor G1 lavas could reflect derivation of their parental melts from an AUM source that was more modified by subduction.

5.7 Reconciling origin of the Erciyes Corridor and Mt. Erciyes lavas with slab rollback

The signature of a deeper-seated, OIB-like mantle component in other CAVP studies has been identified in some volcanic centers (e.g., Kürkcüoglu et al., 1998; Aydin et al., 2014; Reid et al., 2017) and attributed to an asthenospheric component. This component could explain OIB-like trace element concentrations, particularly in more alkaline CAVP basalts, including basaltic lavas erupted at Mt. Erciyes and throughout the CAVP (Kürkcüoglu et al., 2008; Kuscu and Geneli, 2011; Reid et al., 2017). According to the model of slab rollback, involvement of an "asthenospheric" component in melt generation could reflect upwelling of deeper mantle material to fill in behind the Cyprus slab as it foundered under Central Anatolia (Schleiffarth et al., 2018). Reid et al. (2017) postulated that incorporation of this OIB-like component (the IPC) in the Quaternary HMC lavas was driven by slab-rollback-induced convection. The absence of the IPC in the Miocene- to Pliocene Erciyes Corridor basalts and its incorporation in later basalts, such as those at Mt. Erciyes and the HMC, may be due to the progression of slab rollback. In this scenario, the predominantly AUM-sourced Erciyes Corridor basalts would be associated with decompression melting triggered by the initiation of slab rollback. With continued slab rollback, progressively deeper material could be incorporated in magmas, which could explain the chemical signatures of the IPC in Quaternary lavas, such as those from Mt. Erciyes, that are missing in the Erciyes Corridor lavas.

CHAPTER 6: CONCLUSIONS

This study aimed to characterize lavas from the little studied Miocene volcanoes of the Erciyes Corridor in Central Anatolia, Turkey, with the goal of understanding their origins and determining whether a temporal change in source components in the Central Anatolian Volcanic Province occurred. New major- and trace-element geochemistry, isotopic analyses, and petrographic thin sections were interpreted, and the results were compared to previous investigations conducted on volcanic centers across the Central Anatolian Volcanic Province.

The Erciyes Corridor contains both mafic (basaltic) and evolved (basaltic andesite through dacite) lavas, although most of the collected lavas are evolved. Based on chemical and isotopic variations in the Erciyes Corridor lavas, the main outcomes of this thesis research are as follows:

1) Differences in trace element features (e.g., crossing REE patterns) and isotopic characteristics of the Erciyes Corridor basalts and evolved lavas cannot be explained via crystal fractionation ± assimilation from a single source.
2) The evolved lavas of the Erciyes Corridor can be subdivided into two groups based on their isotopic compositions. Group 1 lavas are those with lower $\Delta 7/4$ and $\Delta 8/4$ values and a narrow range in ε_{Hf} values centering around +8, which overlaps the ε_{Hf} values of basalts from the Erciyes Corridor and the Hasan Monogenetic Cluster. These evolved lavas may have differentiated in a closed system via fractional crystallization with negligible contamination by the crust. Crystal fractionation of a mineral assemblage consisting of plagioclase, hornblende, clinopyroxene, orthopyroxene, and titanite could explain the overall change in key trace element concentrations (e.g., La, Sr, Dy, and Yb) from the Group 1 basaltic andesites to the dacites. Judging by their incompatible trace element

characteristics, the parent magmas for Group 1 lavas may reflect contributions from both the ambient upper mantle and subduction-modified mantle components beneath Central Anatolia. These lavas may have been sourced from a basaltic parent comparable to basalts of the Hasan Monogenetic Cluster.

3) Group 2 lavas are those with lower $\boldsymbol{\varepsilon}_{Hf}$ values, ranging from +2.6 to +5.9, and higher $\Delta 7/4$ and $\Delta 8/4$ with respect to the Group 1 lavas. They likely differentiated via crustal assimilation combined with crystal fractionation of plagioclase, hornblende, clinopyroxene, and orthopyroxene, ± titanite. Additionally, the Group 2 evolved lavas exhibit more scatter in their Pb isotopic values and major element concentrations than the Group 1 evolved lavas. Crustal contamination is required to explain the variations in ε_{Hf} values in these lavas and is further supported by a greater decrease in Nb/U with respect to an increase in Th/Yb than can be explained by crystal fractionation.
4) The Erciyes Corridor basalts predominantly reflect melts generated from the ambient upper mantle component under Central Anatolia, likely with little incorporation of a subduction-modified mantle component. This contrasts with other Central Anatolian Volcanic Province basalts, such as those from the Hasan Monogenetic Cluster and from Mt. Erciyes, which reflect greater proportions of contributions from the subduction-modified mantle. Trace element characteristics of the Erciyes Corridor basalts do not require a deeper-seated, OIB-like intraplate mantle component, which has been called upon to explain OIB-like trace element characteristics (e.g., high Ce/Y, low Zr/Nb) in younger Central Anatolian Volcanic Province lavas. The lack of an intraplate mantle component in the Erciyes Corridor basalts may therefore reflect an earlier stage of flat slab rollback under Central Anatolia, with the incorporation of the deeper intraplate

mantle component in later basalts from Mt. Erciyes and the HMC representing the greater progression of rollback-driven convection over time.

APPENDIX

Appendix Table 1: Petrographic thin section descriptions for Erciyes Corridor lavas

CAT16-KS1	Basalt	
Phase	approximate abundance	Notes
Groundmass	10%	Vesicular (irregular shaped vesicles). Diktytaxitic texture. Including crystals that are too altered to be identified or too small.
Plagioclase	60%	Large, elongate crystals with no preferred orientation.
Olivine	20%	Large phenocrysts. Subhedral. Fractured. Abundant iddingsite alteration. Some smaller crystals completely replaced.
Clinopyroxene	5%	Slight color in PPL (tan?), mostly interstitial. 2nd order interference colors,
Orthopyroxene	5%	Few well defined crystals are blocky, subhedral. Most crystals are interstitial--filling in mostly between plagioclase crystals.
CAT15-KS53	G2 Basaltic andesite	
Phase	approximate abundance	Notes
Groundmass	50%	Microlites of major phases; holocrystalline
Plagioclase	25%	Subhedral, elongate crystals. Varying degrees of alteration (sieve texture), no preferred grain orientation; significantly larger than other phenocrysts
Orthopyroxene	10%	Mostly anhedral; some rounded.
Clinopyroxene	10%	Mostly subhedral to anhedral, 2nd order interference colors. Twinning in some crystals, inclined extinction. Some intergrown with opx, oxides
oxides	5%	mostly anhedral; few subhedral crystals

CAT15-KS40	G1 basaltic andesite	
Phase	approximate abundance	Notes
Groundmass	50%	Predominantly plagioclase microlites + few pyroxene fragments. Holocrystalline. Some heavily altered, clay-like material included in groundmass distinction.
Plagioclase	40%	Predominantly subhedral elongate crystals. Sieve texture common. Polysynthetic twinning throughout. Some concentric zoning.
Orthopyroxene	10%	Few elongate crystals with 1st order interference colors. Some with embayments. Parallel extinction.
Clinopyroxene	~1%	One large, rounded crystal with twin. 2nd order interference colors.
oxides	~1%	Very small crystals mostly in groundmass and included in phenocrysts
CAT16-KS49	G2 basaltic andesite	
Phase	approximate abundance	Notes
Groundmass	95%	Trachytic texture composed predominantly of plagioclase laths in glass with lesser fragmented olivine.
Olivine	4%	2nd order interference colors. Subhedral fragments with iddingsite. Fractured.
Orthopyroxene	1%	Very few crystals. 1st order interference colors. Anhedral.

CAT15-KS49	G1 basaltic andesite	
Phase	approximate abundance	Notes
Groundmass	50%	Mostly glassy with fine microlites of major phases. No preferred crystal orientation
Plagioclase	30%	Euhedral to subhedral crystals. Largest overall phase in sample. Twinned.
Clinopyroxene	10%	Heavily opacitized to entirely replaced crystals. Subhedral to anhedral crystals. 2nd order interference colors. Commonly twinned.
Orthopyroxene	5%	Very few crystals. Subhedral. 1st order interference colors.
Oxides	5%	Anhedral crystals. Mostly in groundmass.
CAT16-KS53	G1 basaltic andesite	
Phase	approximate abundance	Notes
Groundmass	~70%	Vesiculated; very fine-grained groundmass material (microlitic),
Olivine	20%	2nd order interference colors; thin rims of iddingsite. Subhedral to anhedral; many broken crystals. Fractures in crystals.
Orthopyroxene	5%	Mostly microlites in groundmass. Few blocky crystals.
plagioclase	5%	Most plagioclase crystals = microlites; few large phenocrysts. Elongate, subhedral crystals. 1st order interference colors.

CAT16-KS47	G2 basaltic andesite	
Phase	approximate abundance	Notes
Groundmass	50%	Heavily altered. Predominantly glass with some yellow clay. No preferred crystal orientation.
Plagioclase	35%	Euhedral to subhedral crystals. Twinned, elongate.
Orthopyroxene	5%	Subhedral crystals. 1st order interference colors.
Clinopyroxene	9%	Heavily fragmented crystals. Some twinning. Some oxide inclusions. Many rounded crystals.
Oxides	1%	Anhedral crystals mostly in groundmass. Some included in major phases.
CAT16-KS16	G2 Andesite	
Phase	approximate abundance	Notes
Groundmass	65%	Glassy with microlites of major phases. Few vesicles. No preferred orientation of microlites.
Plagioclase	25%	Elongate crystals. Commonly zoned. Euhedral to subhedral.
Orthopyroxene	5%	Subhedral/subrounded crystals. 1st order interference colors.
Clinopyroxene	5%	2nd order interference colors. Common twinning. Euhedral to subhedral crystals.
Oxides	~1%	Most common in groundmass.

CAT16-KS54	G1 Andesite	
Phase	approximate abundance	Notes
Groundmass	55%	Predominantly glass with fine plagioclase microlites.
Plagioclase	30%	Euhedral to anhedral. Largest phenocryst in sample. Rare zoning.
Orthopyroxene	10%	1st order crystals. Subhedral, subrounded crystals.
Clinopyroxene	5%	2nd order interference colors. Subhedral crystals. Some twinning. Most crystals heavily fragmented.
Oxides	trace	Fine crystals in groundmass.
CAT16-KS5	G1 Andesite	
Phase	approximate abundance	Notes
Groundmass	99%	Glass with iron staining. Heavily vesiculated.
Plagioclase	1%	Small, elongate crystals. 1st order interference colors. Euhedral.
CAT16-KS21	G2 Dacite	
Phase	approximate abundance	Notes
Groundmass	58%	Glass with fine microlites of plagioclase and oxides. Some iron staining visible in plain light.
Plagioclase	30%	Blocky grains. Twinned. 1st order interference colors.
Clinopyroxene? Hornblende?	2%	2nd order interference colors. Nearly entirely replaced by oxides. Crystal faces not well preserved.
Oxides	10%	Some anhedral crystals. Many retain crystal faces of replaced minerals.

CAT16-KS55	G1 Dacite	
Groundmass	55%	Glassy with fine-grained crystals predominantly of plagioclase. Some irregular vesicles.
Plagioclase	30%	Blocky crystals. Some destroyed cores. Subhedral.
Hornblende	10%	Bright 2nd order interference colors. Mostly fragmented crystals (subhedral to anhedral) with some preserved crystal faces.
Orthopyroxene	5%	Very few crystals. 1st order interference colors.
Oxides	trace	Anhedral crystals mostly in groundmass.

Appendix Table 2: Whole rock geochemical data for Erciyes Corridor lavas

	Basalts					Group 1 (G1)					
Field no.	**CAT16-KS1**	**CAT16-KS18**	**CAT16-KS48**	**CAT16-19**	**R14 HI12**	**CAT15-KS40**	**CAT16-KS53**	**CAT15-KS49**	**CAT16-KS12**	**CAT16-KS54**	**CAT16-KS9**
Volcano	?	Develidag	Erkilet	Koc Dag	Hamurcu	Topuzdag	Hamurcu	Cataltepe	Hamurcu	Hamurcu	Hamurcu
Latitude	38.851139	38.357943	38.877354	38.326276	38.923633	38.770525	38.79822	38.433444	38.722765	38.781964	38.726752
Longitude	35.398722	35.48386	35.41679	35.620037	35.448889	35.000911	35.185825	35.005883	35.211059	35.115341	35.222794
Major element oxides (wt. %, normalized)											
SiO_2	49.51	48.81	49.45	49.45	49.74	54.64	55.98	56.91	57.83	59.34	60.46
TiO_2	1.31	1.91	1.43	1.73	1.58	1.21	1.05	1.09	0.91	0.67	0.83
Al_2O_3	17.62	17.30	17.61	16.85	16.91	18.25	19.37	16.59	18.43	17.89	17.77
Fe_2O_3	11.04	11.33	10.45	11.00	10.74	8.58	8.00	7.32	7.33	5.82	5.37
MnO	0.15	0.17	0.17	0.18	0.16	0.14	0.09	0.08	0.12	0.09	0.09
MgO	7.06	6.73	6.76	6.94	6.45	2.74	1.78	5.18	2.23	4.13	3.06
CaO	9.30	8.73	9.95	9.06	10.15	8.46	7.45	6.70	6.29	7.78	6.27
Na_2O	3.32	3.95	3.50	3.72	3.61	3.81	4.22	4.09	4.44	3.16	3.58
K_2O	0.46	0.69	0.40	0.69	0.42	1.88	1.69	1.76	2.06	0.95	2.35
Cr_2O_3	0.03	0.01	0.06	0.01	0.03	0.00	0.01	0.02	0.00	0.01	0.00
P_2O_5	0.21	0.39	0.22	0.39	0.22	0.30	0.33	0.27	0.36	0.14	0.21
Total	100.00	100.00	100.00	100.00	100.00	100.00	100.00	100.00	100.00	100.00	100.00
Trace Elements (ppm)											
La	17.5	19.3	11.8	17.6	12.3	22	27.9	15.3	28.2	10.9	25.8
Ce	28.7	42.6	18.7	41.1	18.1	45.5	46.4	31.1	58.6	13.6	41.2

Pr	4.2	5.67	3.39	5.28	3.6	5.49	7.28	3.68	7.27	2.71	5.63
Nd	17.4	24.6	14.6	22	15.6	21.5	28.5	14.5	27.8	10.8	20.9
Sm	3.8	5.7	3.6	5.2	4.2	4.6	6.2	3.4	5.6	2.6	4.1
Eu	1.42	1.83	1.42	1.69	1.57	1.38	1.76	1.11	1.5	0.83	1.22
Gd	4.36	6.23	4.3	5.79	4.67	4.66	6.05	3.33	5.81	2.82	4.28
Tb	0.69	1	0.72	0.9	0.8	0.83	0.96	0.6	0.86	0.43	0.68
Dy	4.39	6.28	4.54	5.57	5.02	4.56	5.82	3.09	5.29	2.67	4.15
Ho	0.93	1.27	0.94	1.06	1.07	0.92	1.17	0.61	1.04	0.54	0.86
Er	2.55	3.69	2.67	3.31	3.09	2.81	3.32	1.77	3.26	1.58	2.45
Tm	0.35	0.51	0.37	0.47	0.44	0.45	0.46	0.27	0.44	0.22	0.37
Yb	2.3	3.5	2.5	3	2.8	2.7	3.1	1.6	3.3	1.4	2.5
Lu	0.36	0.47	0.39	0.47	0.42	0.48	0.43	0.29	0.47	0.23	0.37
Ba	261	223	160	215	136	356	318	322	407	497	355
Th	3.4	1.3	2	1.9	2.1	10.5	10.8	5.4	9.9	4.1	12.7
Nb	5.7	10.8	5.1	10	5.4	11	16.3	11	15.4	6.3	15.5
Y	23.3	33.7	24.3	29.5	27.4	27.6	31.2	18.2	29.3	14.8	23.9
Hf	3	5	3	4	4	5	6	4	6	3	6
Ta	0.5	0.6	0.5	0.7	0.5	0.8	0.6	1	0.9	0.5	0.6
U	0.61	0.43	0.39	0.42	0.24	3.15	2.91	2.24	3.19	1.55	4.42
Pb	<5	<5	<5	<5	<5	19	9	11	11	8	13
Rb	6.4	6	5	6.6	4.8	57.6	50.1	43	60.4	30.6	84.3
Cs	0.1	0.2	<0.1	0.1	<0.1	2	1.1	2.7	1.4	1.7	4.8
Sr	445	451	414	455	370	500	535	405	570	404	389
Sc	27	26	30	26	33	20	12	14	9	15	12
Zr	104	237	135	213	140	187	238	139	268	103	223
Radiogenic Isotopes											
$^{176}Hf/^{177}Hf$	0.2829	0.2830	0.2830	0.2830	0.2830	0.2830	0.2830	0.2830	0.2830	0.2831	0.2830
ε_{Hf}	5.6	7.7	7.3	6.9	7.1	8.3	8.8	7.5	8.2	10.1	8.3
$^{206}Pb/^{204}Pb$		18.9632	19.0784	18.9821	19.0593	18.9477	18.9064	18.8853	18.8952	18.8523	18.8976
$^{207}Pb/^{204}Pb$		15.6567	15.6780	15.6708	15.6760	15.6636	15.6592	15.6783	15.6571	15.6708	15.6710
$^{208}Pb/^{204}Pb$		38.9865	39.1657	39.0407	39.1233	39.0036	38.9585	39.0411	38.9511	38.9474	38.9881

Appendix Table 2 (continued)

	Group 1 (G1)						Group 2 (G2)						
Field no.	**CAT16-KS5**	**CAT16-KS13**	**CAT16-KS11**	**CAT16-KS43**	**CAT16-KS21**	**CAT16-KS55**	**CAT16-KS49**	**CAT15-KS54**	**CAT15-KS53**	**CAT16-KS16**	**CAT16-KS22**	**CAT16-KS45**	**CAT16-KS15**
Volcano	Tekgozkopru Ignimbrite	Seksenveren	Hamurcu	Hamurcu	Hoduldag	Seksenveren	Erkilet	Cataltepe	Cataltepe	Develidag	Cataltepe	Erkilet	Koc Dag
Latitude	38.837789	38.659402	38.736707	38.848748	38.51171	38.681726	38.796287	38.493378	38.545372	38.294457	38.520758	38.796287	38.435511
Longitude	35.172153	35.156052	35.218494	35.157444	35.028409	35.167644	35.32716	35.120211	35.062747	35.443352	35.131552	35.32716	35.595297
Major element oxides (wt. %, normalized)													
SiO_2	60.58	60.41	60.32	63.02	67.15	68.88	55.98	56.09	57.22	59.01	64.91	64.57	65.46
TiO_2	1.12	0.78	0.67	1.09	0.34	0.41	1.00	0.90	0.66	0.85	0.48	0.48	0.67
Al_2O_3	17.50	17.26	18.21	18.18	16.51	15.76	17.95	17.39	16.78	18.19	17.21	17.63	15.74
Fe_2O_3	6.19	6.16	5.44	4.84	3.11	3.16	7.27	7.06	6.24	6.74	5.01	4.05	4.43
MnO	0.11	0.09	0.09	0.02	0.05	0.08	0.14	0.10	0.08	0.12	0.09	0.05	0.07
MgO	1.64	2.95	3.60	0.47	1.89	1.16	3.21	5.61	6.06	2.90	2.11	1.77	2.42
CaO	5.28	6.65	6.94	3.52	6.17	3.57	7.26	7.70	8.01	6.60	5.19	4.95	4.55
Na_2O	4.89	3.90	3.40	4.87	3.60	4.14	4.60	3.76	3.47	3.85	3.16	4.00	4.05
K_2O	1.99	1.61	1.18	3.53	1.08	2.74	2.14	1.16	1.30	1.58	1.71	2.36	2.48
Cr_2O_3	0.00	0.01	0.00	0.01	0.00	0.00	0.00	0.02	0.03	0.00	0.00	0.02	0.00
P_2O_5	0.72	0.17	0.14	0.44	0.09	0.09	0.45	0.22	0.15	0.17	0.11	0.12	0.14
Total	100.00	100.00	100.00	100.00	100.00	100.00	100.00	100.00	100.00	100.00	100.00	100.00	100.00
Trace Elements (ppm)													
La	41.6	21.5	11.9	47.1	14.1	26.6	41.7	17.1	19	23.4	18.1	23.6	24.4
Ce	63.1	29.4	17.4	83.8	20.1	38.1	71.2	32.8	35.3	33.5	26.5	35.5	45.6
Pr	9.24	4.18	2.75	10.5	2.76	4.39	8.49	3.8	4.07	5.1	3.65	4.25	5.44
Nd	35.9	15.8	10.7	38.5	9.9	14.5	30.5	14.4	15.1	19.5	13.3	14.8	20
Sm	7.4	3.1	2.4	7.5	1.9	2.4	5.3	3	3.1	4	2.6	2.6	4
Eu	2.17	1	0.72	1.89	0.58	0.76	1.63	1.06	0.99	1.27	0.78	0.77	1.04
Gd	7.92	3.44	2.41	6.98	2.08	2.23	4.89	3.02	2.99	3.97	2.72	2.58	4.06
Tb	1.28	0.56	0.4	1.08	0.31	0.36	0.7	0.51	0.5	0.59	0.44	0.39	0.63
Dy	8.09	3.28	2.32	6.16	1.75	2.07	3.86	2.56	2.65	3.51	2.6	2.27	3.94
Ho	1.8	0.7	0.47	1.27	0.37	0.44	0.8	0.52	0.52	0.71	0.56	0.47	0.76
Er	5.28	2.07	1.31	3.48	1.04	1.29	2.31	1.45	1.55	2.05	1.69	1.39	2.42
Tm	0.77	0.3	0.2	0.49	0.15	0.2	0.32	0.24	0.25	0.28	0.24	0.21	0.35
Yb	5.3	2	1.2	3.2	1	1.4	2.2	1.3	1.4	1.9	1.6	1.4	2.3
Lu	0.84	0.28	0.19	0.47	0.15	0.23	0.33	0.24	0.24	0.3	0.26	0.23	0.38
Ba	437	526	245	690	274	565	668	301	380	583	355	375	418

Th	11	7.9	4.9	20.1	6.7	15.4	12.7	5.2	7.6	7.9	8.9	12.6	15.4
Nb	18.2	9.8	6.9	30.2	4.1	12.6	18.3	9	7	7.5	5.6	10.6	9.2
Y	52.8	21	12.6	33.8	10.1	12.1	22.2	15.4	15.8	19.5	15.3	13.4	21.7
Hf	7	4	3	10	3	4	5	3	4	4	3	4	5
Ta	0.7	0.6	0.5	1.4	0.5	0.6	0.6	0.6	0.6	0.5	0.5	0.5	0.7
U	4.16	2.85	1.79	5.42	1.22	4.48	3.52	1.49	2.07	2.34	2.97	4.04	4.94
Pb	15	8	9	18	11	14	11	8	11	11	11	13	12
Rb	67.5	48.1	35.9	117	22.5	90.3	53.3	25.5	41.5	47.4	65.3	92.4	85.9
Cs	4.4	1	2	2.7	0.3	2.4	53.3	25.5	41.5	47.4	65.3	92.4	85.9
Sr	398	392	445	317	289	265	795	444	364	464	263	366	283
Sc	10	14	12	9	8	6	10	18	18	15	11	7	10
Zr	244	145	108	422	90.2	151	213	110	131	134	117	144	216
Radiogenic Isotopes													
$^{176}Hf/^{177}Hf$	0.2830	0.2830	0.2830	0.2830	0.2830	0.2830	0.2828	0.2829	0.2829	0.2828	0.2829	0.2829	0.2829
ε_{Hf}	8.4	8.4	8.4	8.0	8.5	7.9	2.6	5.3	4.8	2.6	5.9	4.3	5.9
$^{206}Pb/^{204}Pb$	18.9110	18.8784	18.8623	18.8996	18.8272	18.9047	18.9204	18.9431	18.8792	18.9481	18.8532	18.9441	18.9527
$^{207}Pb/^{204}Pb$	15.6694	15.6674	15.6749	15.6591	15.6783	15.6734	15.6773	15.6925	15.6859	15.6828	15.6864	15.6996	15.6824
$^{208}Pb/^{204}Pb$	38.9919	38.9811	38.9759	38.9656	39.0067	39.0060	38.9875	39.1057	39.1102	39.0709	39.0332	39.1509	39.1036

Appendix Table 3: Partition coefficients used for crystal fractionation modeling.

Element	Olivine (1)	Orthopyroxene (1)	Clinopyroxene (1)	Hornblende (2)	Plagioclase (2)	Titanite (2)	Apatite (1)
Rb	0.0098	0.022	0.02	0	0.01	0.01	
Ba	0.0099	0.013	0.02	0.08	0.61		
Th			0.01	0.01	0.001	18.7	
U	0.002		0.21	0.01	0.019	7	
Nb	0.01	0.15	0.173	2	0.001	129	0.1
Ta				0.5	0.001	153	
K	0.0068	0.014	0.02		0.263		
La	0.0067		0.047	1.4	0.4	113	14.5
Ce	0.006	0.028	0.084	3.2	0.3	223	21.1
Pb				0.1	0.5	0.1	
Pr						419	
Sr	0.014	0.04	0.08	0.4	12.5	0.37	
P							
Nd	0.0059	0.006	0.183	9.7	0.2	639	32.8
Zr	0.012	0.18	0.162	0.5		9.64	0.73
Hf	0.013		0.162	0.9		18.7	0.1
Sm	0.007	0.012	0.377	15.5	0.1	930	46
Eu	0.0074	0.024	0.8	10.8	3.1	661	25.5
Ti	0.02	0.1	0.4	7	0.05		
Gd	0.01	0.09	0.583	14.9	0.08	855	43.9
Tb		0.06				1231	
Dy	0.013	0.15	0.774	17.6	0.02	935	47.4
Ho						884	
Y	0.01	0.18	1.5	13.5	0.02	633	
Er	0.0256	0.13	0.708	13.2	0.001	636	22.7
Yb	0.0491	0.2	0.633	9.6	0.01	393	15.4
Lu	0.0454	0.22	0.665	5	0.062	237	13.8
Cr	0.7	10	30	20.6	5.4		189.5
Ni	17	5	6	45	2.8	0.26	

(1) Rollinson, 1993
(2) Bachmann et al., 2005

REFERENCES

Abgarmi, B., Delph, J.R., Arda Ozacar, A., Beck, S.L., Zandt, G., Sandvol, E., Turkelli, N., and Biryol, C.B., 2017, Structure of the crust and African slab beneath the central Anatolian plateau from receiver functions: New insights on isostatic compensation and slab dynamics: Geosphere, v. 13, p. 1774–1787, doi:10.1130/GES01509.1.

Aldanmaz, E., Pickard, M., Meisel, T., Altunkaynak, Ş., Sayıt, K., Şen, P., Hanan, B.B., and Furman, T., 2015, Source components and magmatic processes in the genesis of Miocene to Quaternary lavas in western Turkey: constraints from HSE distribution and Hf–Pb–Os isotopes: Contributions to Mineralogy and Petrology, v. 170, doi:10.1007/s00410-015-1176-x.

Alici, P., Temel, A., and Gourgaud, A., 2002, Pb-Nd-Sr isotope and trace element geochemistry of Quaternary extension-related alkaline volcanism: A case study of Kula region (western Anatolia, Turkey): Journal of Volcanology and Geothermal Research, v. 115, p. 487–510, doi:10.1016/S0377-0273(01)00328-6.

Arger, J., Mitchell, J., and Westaway, R.W.C., 2000, Neogene and Quaternary volcanism of southeastern Turkey: Geological Society Special Publication, v. 173, p. 459–487, doi:10.1144/GSL.SP.2000.173.01.22.

Aydar, E., Gourgaud, A., Deniel, C., Lyberis, N., and Gundogdu, N., 1995, Le volcanisme quaternaire d'Anatolie centrale (Turquie): association de magmatismes calco-alcalin et alcalin en domaine de convergence: Canadian Journal of Earth Sciences, v. 32, p. 1058–1069, doi:10.1139/e95-087.

Aydar, E., Çubukçu, H.E., Şen, E., and Akin, L., 2013, Central Anatolian Plateau, Turkey: Incision and paleoaltimetry recorded from volcanic rocks: Turkish Journal of Earth Sciences, v. 22, p. 739–746, doi:10.3906/yer-1211-8.

Akin, L., Aydar, E., Schmitt, A.K., Çubukçu, H.E., and Gerdes, A., 2021, Zircon geochronology and O-Hf isotopes of Cappadocian ignimbrites: New insights into continental crustal architecture underneath the Central Anatolian Volcanic Province, Turkey: Gondwana Research, v. 91, p. 166–187, doi:10.1016/j.gr.2020.12.003.

Aydin, F., Schmitt, A.K., Siebel, W., Sönmez, M., Ersoy, Y., Lermi, A., Dirik, K., and Duncan, R., 2014, Quaternary bimodal volcanism in the Niğde Volcanic Complex (Cappadocia, central Anatolia, Turkey): age, petrogenesis and geodynamic implications: Contributions to Mineralogy and Petrology, v. 168, p. 1–24, doi:10.1007/s00410-014-1078-3.

Bachmann, O., Dungan, M.A., and Bussy, F., 2005, Insights into shallow magmatic processes in large silicic magma bodies: The trace element record in the Fish Canyon magma body, Colorado: Contributions to Mineralogy and Petrology, v. 149, p. 338–349, doi:10.1007/s00410-005-0653-z.

Bartol, J., and Govers, R., 2014, A single cause for uplift of the Central and Eastern Anatolian plateau? Tectonophysics, v. 637, p. 116–136, doi:10.1016/j.tecto.2014.10.002.

Berk Biryol, C., Beck, S.L., Zandt, G., and Özacar, A.A., 2011, Segmented African lithosphere beneath the Anatolian region inferred from teleseismic P-wave tomography: Geophysical Journal International, v. 184, p. 1037–1057, doi:10.1111/j.1365-246X.2010.04910.x.

Chakrabarti, R., A. R. Basu, and A. Ghatak (2012), Chemical geodynamics of western Anatolia, Int. Geol. Rev., 54(2), 227–248.

Colombini, L.L., Miller, C.F., Gualda, G.A.R., Wooden, J.L., and Miller, J.S., 2011, Sphene and zircon in the Highland Range volcanic sequence (Miocene, southern Nevada, USA): Elemental partitioning, phase relations, and influence on evolution of silicic magma: Mineralogy and Petrology, v. 102, p. 29–50, doi:10.1007/s00710-011-0177-3.

Darin, M.H., Umhoefer, P.J., and Thomson, S.N., 2018, Rapid Late Eocene Exhumation of the Sivas Basin (Central Anatolia) Driven by Initial Arabia-Eurasia Collision: Tectonics, v. 37, p. 3805–3833, doi:10.1029/2017TC004954.

Davidson, J., Turner, S., and Plank, T., 2013, Dy/Dy*: Variations arising from mantle sources and petrogenetic processes: Journal of Petrology, v. 54, p. 525–537, doi:10.1093/petrology/egs076.

Deniel, C., Aydar, E., and Gourgaud, A., 1998, The Hasan Dagi stratovolcano (Central Anatolia, Turkey): Evolution from calc-alkaline to alkaline magmatism in a collision zone: Journal of Volcanology and Geothermal Research, v. 87, p. 275–302, doi:10.1016/S0377-0273(98)00097-3.

Dogan, A.U., Peate, D.W., Dogan, M., Yesilyurt-Yenice, F.I., and Unsal, O., 2013, Petrogenesis of mafic-silicic lavas at Mt. Erciyes, central Anatolia, Turkey: Journal of Volcanology and Geothermal Research, v. 256, p. 16–28, doi:10.1016/j.jvolgeores.2013.01.020.

Dogan-Kulahci, G.D., Temel, A., Gourgaud, A., Varol, E., Guillou, H., and Deniel, C., 2018, Contemporaneous alkaline and calc-alkaline series in Central Anatolia (Turkey): Spatio-temporal evolution of a post-collisional Quaternary basaltic volcanism: Journal of Volcanology and Geothermal Research, v. 356, p. 56–74, doi:10.1016/j.jvolgeores.2018.02.012.

Gualda, G.A.R., Gravley, D.M., Deering, C.D., and Ghiorso, M.S., 2019, Magma extraction pressures and the architecture of volcanic plumbing systems: Earth and Planetary Science Letters, v. 522, p. 118–124, doi:10.1016/j.epsl.2019.06.020.

Gürsoy, H., Tatar, O., Piper, J.D.A., Koçbulut, F., Akpinar, Z., Huang, B., Roberts, A.P., and Mesci, B.L., 2011, Palaeomagnetic study of the Kepezdaĝ and Yamadaĝ volcanic complexes, central Turkey: Neogene tectonic escape and block definition in the central-east Anatolides: Journal of Geodynamics, v. 51, p. 308–326, doi:10.1016/j.jog.2010.07.004.

Hanan, B.B., and Graham, D.W., 1996, Lead and Helium Isotope Evidence from Oceanic Basalts for a Common Deep Source of Mantle Plumes Author (s): B . B . Hanan and D . W . Graham Published by : American Association for the Advancement of Science Stable URL : http://www.jstor.org/stable/2889: Science, v. 272, p. 991–995.

Hart, S.R., 1984, A large-scale isotope anomaly in the Southern Hemisphere mantle: Nature, v. 309, p. 753–757.

Innocenti, F., Mazzuoli, R., Pasquarè, G., Radicati di Brozolo, F., and Villari, L., 1975, The Neogene calcalkaline volcanism of Central Anatolia: Geochronological data on Kayseri—Nigde area: Geological Magazine, v. 112, p. 349–360, doi:10.1017/S0016756800046744.

Klaver, M., Djuly, T., de Graaf, S., Sakes, A., Wijbrans, J., Davies, G., and Vroon, P., 2015, Temporal and spatial variations in provenance of Eastern Mediterranean Sea sediments: Implications for Aegean and Aeolian arc volcanism: Geochimica et Cosmochimica Acta, v. 153, p. 149–168, doi:10.1016/j.gca.2015.01.007.

Kohn, M.J., 2017, Titanite Petrochronology: Reviews in Mineralogy and Geochemistry, v. 83, p. 419–441, doi:10.2138/rmg.2017.83.13.

Kürkcüoglu, B., 2010, Geochemistry and petrogenesis of basaltic rocks from the Develidağ volcanic complex, Central Anatolia, Turkey: Journal of Asian Earth Sciences, v. 37, p. 42–51, doi:10.1016/j.jseaes.2009.07.004.

Kürkçüoglu, B., Sen, E., Aydar, E., Gourgaud, A., and Gündogdu, N., 1998, Geochemical approach to magmatic evolution of Mt. Erciyes stratovolcano Central Anatolia, Turkey: Journal of Volcanology and Geothermal Research, v. 85, p. 473–494, doi:10.1016/S0377-0273(98)00067-5.

Kurt, H., Asan, K., and Ruffet, G., 2008, The relationship between collision-related calcalkaline, and within-plate alkaline volcanism in the Karacadağ Area (Konya-Türkiye, Central Anatolia): Chemie der Erde, v. 68, p. 155–176, doi:10.1016/j.chemer.2006.05.003.

Kuscu, G., 2011, Geochemical characterization of a Quaternary monogenetic volcano in Erciyes Volcanic Complex: Cora Maar (Central Anatolian Volcanic Province, Turkey): International Journal of Earth Sciences, v. 100, p. 1967–1985, doi:10.1007/s00531-010-0620-4.

Kuscu, G.G., and Geneli, F., 2010, Review of post-collisional volcanism in the Central Anatolian Volcanic Province (Turkey), with special reference to the Tepekoy Volcanic Complex:

International Journal of Earth Sciences, v. 99, p. 593–621, doi:10.1007/s00531-008-0402-4.

Le Bas, M.J., Le Maitre, R.W., Streckeisen, A., and Zanettin, B., 1986, A chemical classification of volcanic rocks based on the total alkali-silica diagram: Journal of Petrology, v. 27, p. 745–750, doi:10.1093/petrology/27.3.745.

Le Pennec, J.L., Bourdier, J.L., Froger, J.L., Temel, A., Camus, G., and Gourgaud, A., 1994, Neogene ignimbrites of the Nevsehir plateau (Central Turkey): stratigraphy, distribution and source constraints: Journal of Volcanology and Geothermal Research, v. 63, p. 59–87, doi:10.1016/0377-0273(94)90018-3.

Lustrino, M., and Wilson, M., 2007, The circum-Mediterranean anorogenic Cenozoic igneous province: Earth-Science Reviews, v. 81, p. 1–65, doi:10.1016/j.earscirev.2006.09.002.

McNab, F., Ball, P.W., Hoggard, M.J., and White, N.J., 2018, Neogene Uplift and Magmatism of Anatolia: Insights From Drainage Analysis and Basaltic Geochemistry: Geochemistry, Geophysics, Geosystems, v. 19, p. 175–213, doi:10.1002/2017GC007251.

Meijers, M.J.M., Brocard, G.Y., Cosca, M.A., Lüdecke, T., Teyssier, C., Whitney, D.L., and Mulch, A., 2018, Rapid late Miocene surface uplift of the Central Anatolian Plateau margin: Earth and Planetary Science Letters, v. 497, p. 29–41, doi:10.1016/j.epsl.2018.05.040.

Notsu, K., Fujitani, T., Ui, T., Matsuda, J., and Ercan, T., 1995, Geochemical features of collision-related volcanic rocks in central and eastern Anatolia, Turkey: Journal of Volcanology and Geothermal Research, v. 64, p. 171–191, doi:10.1016/0377-0273(94)00077-T.

Pearce, J.A., Bender, J.F., De Long, S.E., Kidd, W.S.F., Low, P.J., Güner, Y., Saroglu, F., Yilmaz, Y., Moorbath, S., and Mitchell, J.G., 1990, Genesis of collision volcanism in Eastern Anatolia, Turkey: Journal of Volcanology and Geothermal Research, v. 44, p. 189–229, doi:10.1016/0377-0273(90)90018-B.

Pearce, J.A., Stern, R.J., Bloomer, S.H., and Fryer, P., 2005, Geochemical mapping of the Mariana arc-basin system: Implications for the nature and distribution of subduction components: Geochemistry, Geophysics, Geosystems, v. 6, doi:10.1029/2004GC000895.

Portner, D.E., Delph, J.R., Berk Biryol, C., Beck, S.L., Zandt, G., Özacar, A.A., Sandvol, E., and Türkelli, N., 2018, Subduction termination through progressive slab deformation across Eastern Mediterranean subduction zones from updated P-wave tomography beneath Anatolia: Geosphere, v. 14, p. 907–925, doi:10.1130/GES01617.1.

Reilinger, R. et al., 2006, GPS constraints on continental deformation in the Africa-Arabia-Eurasia continental collision zone and implications for the dynamics of plate interactions: Journal of Geophysical Research: Solid Earth, v. 111, p. 1–26, doi:10.1029/2005JB004051.

Reid, M.R., Delph, J.R., Cosca, M.A., Schleiffarth, W.K., and Gençalioğlu Kuşcu, G., 2019, Melt equilibration depths as sensors of lithospheric thickness during Eurasia-Arabia collision and the uplift of the Anatolian Plateau: Geology, v. 47, p. 943–947, doi:10.1130/G46420.1.

Reid, M.R., Schleiffarth, W.K., Cosca, M.A., Delph, J.R., Blichert-Toft, J., and Cooper, K.M., 2017, Shallow melting of MORB-like mantle under hot continental lithosphere, Central Anatolia: Geochemistry, Geophysics, Geosystems, v. 18, p. 1–23, doi:10.1002/2016GC006772.

Rudnick, R.L., and Gao, S., 2013, Composition of the Continental Crust, *in* Treatise on Geochemistry: Second Edition, Elsevier Ltd., v. 4, p. 1–51, doi:10.1016/B978-0-08-095975-7.00301-6.

Schleiffarth, W.K., Darin, M.H., Reid, M.R., and Umhoefer, P.J., 2018, Dynamics of episodic Late Cretaceous-Cenozoic magmatism across Central to Eastern Anatolia: New insights from an extensive geochronology compilation: Geosphere, v. 14, p. 1990–2008, doi:10.1130/GES01647.1.

Schleiffarth, W.K., 2018, The origins and spatial-temporal patterns of Cretaceous-Quaternary magmatism during collisions, trench retreat, and escape tectonics in Central Anatolia, Turkey [Ph.D thesis]: Northern Arizona University, 151 p.

Schmitt, A.K., Danišík, M., Evans, N.J., Siebel, W., Kiemele, E., Aydin, F., and Harvey, J.C., 2011, Acigöl rhyolite field, Central Anatolia (part 1): High-resolution dating of eruption episodes and zircon growth rates: Contributions to Mineralogy and Petrology, v. 162, p. 1215–1231, doi:10.1007/s00410-011-0648-x.

Sengor, A.M.C., Gorur, N., and Saroglu, F., 1985, Strike-slip faulting and related basin formation in zones of tectonic escape: Turkey as a case study.: Strike-slip deformation, basin formation, and sedimentation, v. 37, p. 227–264, doi:10.2110/pec.85.37.0227.

Sun, S. S., and W. S. McDonough (1989), Chemical and isotopic systematics of oceanic basalts: Implications for mantle composition and processes, Geol. Soc. Spec. Publ., 42(1), 313–345.

Temel, A., Gundogdu, M.N., and Gourgaud, A., 1998, Petrological and geochemical characteristics of Cenozoic high-K calc-alkaline volcanism in Konya , Central Anatolia , Turkey:

Temel, A., Gündogdu, M.N., Gourgaud, A., and Le Pennec, J.L., 1998, Ignimbrites of Cappadocia (Central Anatolia, Turkey): Petrology and geochemistry: Journal of Volcanology and Geothermal Research, v. 85, p. 447–471, doi:10.1016/S0377-0273(98)00066-3.

Toprak, V., 1998, Vent distribution and its relation to regional tectonics, Cappadocian Volcanics, Turkey: Journal of Volcanology and Geothermal Research, v. 85, p. 55–67, doi:10.1016/S0377-0273(98)00049-3.

Uslular, G., and Gençalioğlu-Kuşcu, G., 2019, Geochemical Characteristics of Anatolian Basalts: Comment on "Neogene Uplift and Magmatism of Anatolia: Insights From Drainage Analysis and Basaltic Geochemistry" by McNab Et Al.: Geochemistry, Geophysics, Geosystems, v. 20, p. 530–541, doi:10.1029/2018GC007533.

Van Hunen, J., and Miller, M.S., 2015, Collisional processes and links to episodic changes in subduction zones: Elements, v. 11, p. 119–124, doi:10.2113/gselements.11.2.119.

White, W.M., 2017, Geochemistry, *in* White, W.M. ed., Encyclopedia of Geochemistry: A Comprehensive Reference Source on the Chemistry of the Earth, Cham, Springer International Publishing, p. 1–10, doi:10.1007/978-3-319-39193-9_294-1.

Xirouchakis, D., Lindsley, D.H., and Frost, B.R., 2001, Assemblages with titanite (CaTiOSiO4), Ca-Mg-Fe olivine and pyroxenes, Fe-Mg-Ti oxides, and quartz: Part II. Application: American Mineralogist, v. 86, p. 254–264, doi:10.2138/am-2001-2-307.